TADF-Based NIR-II Semiconducting Polymer Dots for In Vivo 3D Bone Imaging

Keng-Fang Hsu,[a†] Shih-Po Su,[b†] Hsiu-Feng Lu,[cd†] Ming-Ho Liu,[a] Yuan Jay Chang,[e] Yi-Jang Lee,[f] Huihua Kenny Chiang,[b] Chao-Ping Hsu,[cd] Chin-Wei Lu,[g]* and Yang-Hsiang Chan[ahi]**

[a.] *Department of Applied Chemistry, National Yang Ming Chiao Tung University, Hsinchu, Taiwan 30050.*
[b.] *Institute of Biomedical Engineering, National Yang Ming Chiao Tung University, Taipei, Taiwan 11221.*
[c.] *Institute of Chemistry, Academia Sinica, 128 Section 2, Academia Road, Nankang, Taipei 115, Taiwan.*
[d.] *National Center for Theoretical Sciences, 1, Section 4, Roosevelt Road, Taipei 106, Taiwan*
[e.] *Department of Chemistry, Tunghai University, Taichung City 40704, Taiwan*
[f.] *Department of Biomedical Imaging and Radiological Sciences, School of Biomedical Engineering, National Yang Ming Chiao Tung University, Taipei, Taiwan 11221.*
[g.] *Department of Applied Chemistry, Providence University, Taichung 43301, Taiwan.*
[h.] *Center for Emergent Functional Matter Science, National Yang Ming Chiao Tung University, Hsinchu, Taiwan 30010.*
[i.] *Department of Medicinal and Applied Chemistry, Kaohsiung Medical University, Kaohsiung, Taiwan 80708.*
† Authors contributed equally to this work.

Supplementary Information

Table of Contents

Experimental Section **S3**

Synthesis and Characterization **S3**

Supplementray Figures **S13**

NMR Spectra **S24**

Supplementary References **S40**

Experimental Procedures

Materials. The chemicals used in the experiments were purchased from Alfa Aesar, Sigma-Aldrich, TCI, and Acros. All chemicals were used as received unless described otherwise. All bio-related agents such as streptavidin, antibody, or medium are purchased form Life Technologies (Thermo Fisher Scientific). Phospholipids including mPEG-DPSE (M_w=2000) and DOPG sodium salt were obtained from Laysan Bio, Inc or TCI. High purity water (18.2 MΩ•cm) was used throughout the experiment. All ^{1}HNMR and ^{13}CNMR spectra were recorded on a Bruker AVIII HD 400 spectrometer (400 MHz). Compound 1,[1] 9,[2] ,11-12,[3] T3,[3] 13,[4] and T4[4] were synthesized according to the reported literatures.

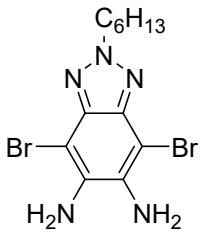

2

4,7-dibromo-2-hexyl-2H-benzo[d][1,2,3]triazole-5,6-diamine, ***2*** Compound **1** (0.9 g, 2.0 mmol) and iron powder (1.7 g, 30.4 mmol) were added into a round-bottomed flask and then dissolved in 20 mL of glacial acetic acid. The mixture was stirred at 40 °C for 2 h. Afterward, iron powder was removed and then Na_2HCO_3 solution was added to titrate acetic acid to pH ~7. The residue was dissolved in CH_2Cl_2 to extract with brine for three times. After dried by anhydrous $MgSO_4$, the solvent was removed under reduced pressure and the product was collected without further purification for the next step immediately.

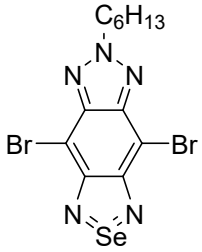

3

Compound ***3*** Compound **2** (640 mg, 1.6 mmol) was added into a two-neck round-bottom flask and then 9.6 mL of ethanol was added to dissolve compound **2**. For another flask, SeO_2 (0.2 g, 1.7 mmol) was dissolved in 3.4 mL of water and then added into the above a two-neck round-bottom flask. The mixture was heated to 70 °C and stirred for 3 h. Afterward, the mixture was poured into 30 mL of ice water for the solid to precipitate out. The solid was collected and rinsed with copious ice water. After that, the residue was dissolved in CH_2Cl_2 to extract with brine for three times. After dried by anhydrous $MgSO_4$, the solvent was removed under reduced pressure and the product was purified by column chromatography on silica gel with CH_2Cl_2 as eluent to get 712 mg (76%) of compound **3** as a red-purple solid. ^{1}H NMR (400 MHz, $CDCl_3$) δ = 4.89 (t, J = 7.8 Hz, 2H), 2.28

(quin, *J* = 7.4 Hz 2H), 1.49-1.33 (m, 6H), 0.90 (t, *J* = 6.7 Hz, 3H). ^{13}C NMR (101 MHz, $CDCl_3$) δ = 156.91, 146.29, 99.80, 59.43, 31.24, 30.28, 26.37, 22.52, 14.07. HRMS (FD, [M]) for C12H13N5SeBr2 calcd. 464.8708, found: 466.8709.

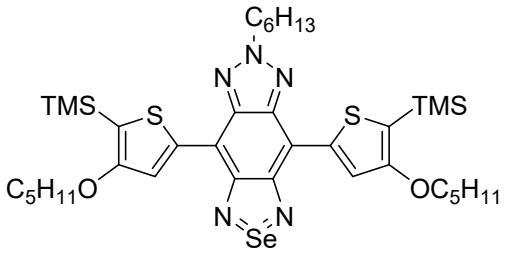

4

<u>*Compound **4***</u> Compound **3** (1.46 g, 2.15 mmol), trimethyl(3-(pentyloxy)-5-(tributylstannyl)thiophen-2-yl)silane (500 mg, 1.07 mmol), $Pd(PPh_3)_2Cl_2$ (75 mg, 0.11 mmol), and 20 mL of dry THF were added into a round-bottom flask under nitrogen atmosphere and then the mixture was heated to 85 °C for 48 h with stirring. After the reaction, CH_2Cl_2 was added to extract with brine for three times. After dried by anhydrous $MgSO_4$, the solvent was removed under reduced pressure and the product was purified by column chromatography on aluminum oxide with hexane/ ethyl acetate (10:1, v/v) as eluent to get 180 mg (21%) of compound **4** as an oil. ^{1}H NMR (400 MHz, C_6D_6) δ = 9.10 (s, 2H), 4.37 (t, *J* = 7.1 Hz, 2H), 4.19 (t, *J* = 6.5 Hz, 4H), 1.90 (d, *J* = 7.3 Hz, 2H), 1.75 (quin, *J* = 6.5 Hz, 4H), 1.46 - 1.27 (m, 14H), 0.89 (t, *J* = 7.3 Hz, 6H), 0.85 - 0.79 (m, 3H), 0.59 (s, 18H). ^{13}C NMR (101 MHz, C_6D_6) δ = 164.80, 156.73, 143.73, 142.07, 120.85, 120.43, 112.48, 71.29, 57.96, 31.48, 30.23, 29.89, 28.72, 26.49, 22.82, 22.76, 14.30, 14.21, 1.42, 0.11. HRMS (FD, [M]) for C36H55O2Si2S2Se calcd. 789.2506, found: 789.2513.

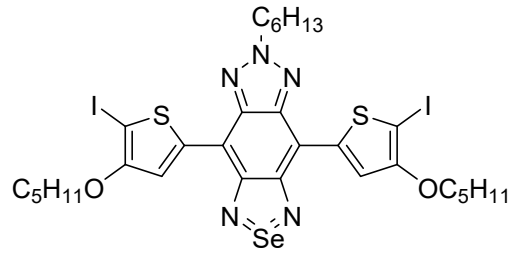

SBO

<u>*Compound **SBO***</u> Compound **4** (50 mg, 0.06 mmol) was first dissolved in 4 mL of THF in a round-bottom flask covered by aluminum foil. *N*-iodosuccinimide (31.36 mg, 0.14 mmol) dissolved in 10 mL of THF was then slowly added by dropping funnel and stirred for 1 h at 0 °C. After the reaction, 5 mL of CH_2Cl_2 was added and then 10 % of $Na_2S_2O_3$ aqueous solution was added into the solution to quench the unreacted *n*-iodosuccinimide. The organic layer was separated and extracted with saturated Na_2CO_3 solution for three times. After dried by anhydrous $MgSO_4$, the organic solvent was removed under reduced pressure and the product was purified by short column chromatography on basic aluminum oxide with CH_2Cl_2 as eluent to get 51 mg (90%) of compound **SBO** as a dark-green solid. ^{1}H NMR (400 MHz, C_6D_6) δ = 8.62 (s, 2H), 4.39 (t, *J* = 7.3 Hz, 2H), 4.14 (t, *J* = 6.5 Hz, 4H), 1.90 (quin, *J* = 7.1 Hz, 2H), 1.77 (quin, *J* = 6.7 Hz, 4H), 1.48 - 1.26 (m, 14H), 0.91 (t, *J* = 7.2 Hz, 6H), 0.86 (t, *J* = 6.7 Hz, 3H). ^{13}C NMR (101 MHz, C_6D_6) δ = 160.51, 155.94, 143.06, 142.37, 125.42, 119.54, 111.88, 72.31, 64.60, 58.11,

31.47, 30.52, 30.49, 30.22, 29.91, 29.82, 29.71, 28.54, 26.53, 22.86, 22.83, 14.31, 14.24, 1.42. HRMS (FD, [M]) for C30H37N5O2S2SeI2 calcd. 896.9649, found: 896.9661.

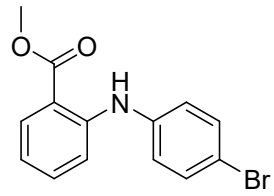

5

*Methyl 2-((4-bromophenyl)amino)benzoate, **5**.* 1-bromo-4-iodobenzene (1.09 g, 3.86 mmol), copper powder (0.005 g, 0.08 mmol), and 2-carbomethoxyaniline (0.5 mL, 3.86 mmol) were added into a round-bottom flask under nitrogen atmosphere. 9.56 mL of 1,2-dichlorobenzene was then added to dissolve the reagents and then heated under reflux (ca. 190 °C) for 48 h. After the reaction, copper was removed and the solvent was removed under reduced pressure. Ethyl acetate was then added into the solution to extract with brine for three times. After dried by anhydrous $MgSO_4$, the solvent was removed under reduced pressure and the product was purified by column chromatography on silica gel with hexane as eluent to afford 550 mg (47%) of compound **5**. ^{1}H NMR (400 MHz, $CDCl_3$) δ = 9.44 (s, 1H), 7.96 (d, *J* = 1.1 Hz, 1H), 7.43 (d, *J* = 8.7 Hz, 2H), 7.33 (t, *J* = 7.8 Hz, 1H), 7.22 (d, *J* = 8.5 Hz, 1H), 7.12 (d, *J* = 8.7 Hz, 2H), 6.77 (t, *J* = 7.5 Hz, 1H), 3.91 (s, 3H). ^{13}C NMR (101 MHz, $CDCl_3$) δ = 169.01, 147.42, 140.12, 134.30, 132.47, 131.83, 123.86, 117.81, 115.89, 114.20, 112.51, 51.99. HRMS (FD, [M]) for C14H12NO2Br calcd. 305.0057, found: 305.0052.

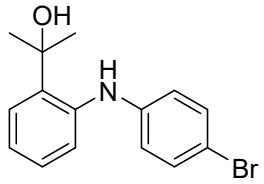

6

*2-(2-((4-bromophenyl)amino)phenyl)propan-2-ol, **6**.* Compound **5** (550 mg, 1.80 mmol) and added into a round-bottom flask under nitrogen atmosphere. 5.44 mL of THF was then added at 0 °C, followed by the addition of methylmagnesium bromide (3.0 M, 1.80 mL, 1.80 mmol). The mixture was stirred for 1 h at room temperature. After the reaction, water was added to quench the reaction and then ethyl acetate was added to extract with water. The organic layer was separated and extracted with brine for three times. After dried by anhydrous $MgSO_4$, the organic solvent was removed under reduced pressure to afford 300 mg (55%) of compound **6**. ^{1}H NMR (400 MHz, $(CD_3)_2SO$) δ = 8.50 (s, 1H), 7.34 (d, *J* = 8.8 Hz, 2H), 7.30 (dd, *J* = 7.8, 1.5 Hz, 1H), 7.23 (dd, *J* = 8.0, 1.5 Hz, 1H), 7.17 (td, *J* = 8.0, 7.6, 1.5 Hz, 1H), 6.91 - 6.88 (m, 1H), 5.79 (s, 1H), 1.50 (s, 6H). ^{13}C NMR (101 MHz, $(CD_3)_2SO$) δ = 143.55, 140.97, 137.21, 131.95, 127.44, 126.08, 121.04, 119.65, 117.84, 109.96, 72.23, 29.66. HRMS (FD, [M]) for C15H16NOBr calcd. 305.0421, found: 305.0431.

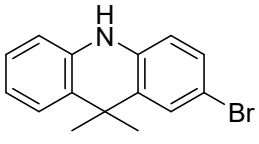

7

2-bromo-9,9-dimethyl-9,10-dihydroacridine, 7. Compound **6** (300 mg, 0.99 mmol) and phosphoric acid (1.49 mL，25.6 mmol) were added into a round-

bottom flask and stirred for 3 h at room temperature. Afterward, ethyl acetate was added to extract with brine for three times. After dried by anhydrous $MgSO_4$, the organic solvent was removed under reduced pressure and the product was purified by column chromatography on silica gel with hexane as to afford 260 mg (95%) of compound **7**. ^{1}H NMR (400 MHz, $(CD_3)_2SO$) δ = 9.00 (s, 1H), 7.45 (d, *J* = 2.3 Hz, 1H), 7.34 (dd, *J* = 7.8, 1.5 Hz, 1H), 7.20 (dd, *J* = 8.5, 2.2 Hz, 1H), 7.06 (td, *J* = 7.5, 1.4 Hz, 1H), 6.85-6.73 (m, 30H), 1.47 (s, 6H). ^{13}C NMR (101 MHz, $(CD_3)_2SO$) δ = 138.11, 138.08, 130.54, 129.30, 128.05, 127.53, 126.78, 125.50, 119.97, 115.34, 113.46, 110.53, 35.85, 31.04. HRMS (FD, [M]) for C15H14NBr calcd. 287.0315, found: 287.0318.

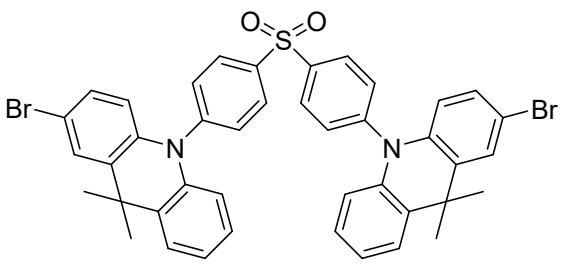

T1

*10,10'-(sulfonylbis(4,1-phenylene))bis(2-bromo-9,9-dimethyl-9,10-dihydroacridine), **T1**.* Compound **7** (0.30 g, 1.04 mmol) and NaH (50 mg, 1.08 mmol) were added into a two-neck round-bottom flask under nitrogen atmosphere, and 30 mL of dry DMF was added. For the other flask, bis(4-fluorophenyl) sulfone (0.13 g，5.20 mmol) dissolved in dry DMF was added into the above flask. The solution was heated to 100 °C under reflux and stirred for 1 h. Afterward, ethyl acetate and water were added and the organic layer was separated to further extract with brine for three times. After dried by anhydrous $MgSO_4$, the solvent was removed under reduced pressure and the product was purified by column chromatography on silica gel with hexane/ethyl acetate (4:1, v/v) as eluent to get 0.12 g (60%) of compound **T1**. ^{1}H NMR (400 MHz, $CDCl_3$) δ = 8.27 (d, *J* = 8.5 Hz, 4H), 7.55 (dd, *J* = 5.4, 3.1 Hz, 6H), 7.50 - 7.44 (m, 2H), 7.10 (dd, *J* = 8.8, 2.2 Hz, 2H), 7.06 - 6.97 (m, 4H), 6.35 - 6.25 (m, 2H), 6.18 (d, *J* = 8.8 Hz, 2H), 1.65 (s, 12H). ^{13}C NMR (101 MHz, $CDCl_3$) δ = 146.60, 140.65, 140.03, 133.96, 131.21, 130.83, 129.42, 128.57, 126.84, 125.58, 122.27, 116.64, 115.12, 114.41, 36.54, 30.85. HRMS (FD, [M]) for C42H34N2O2SBr2 calcd. 788.0713, found: 788.0704.

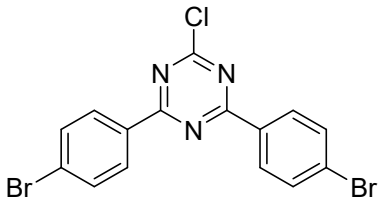

8

*2,4-bis(4-bromophenyl)-6-chloro-1,3,5-triazine, **8**.* 1-bromo-4-iodobenzene (3.53 g， 12.47 mmol) was added into a flask under nitrogen atmosphere and then 62 mL of diethyl ether was added at -78 °C, followed by the dropwise addition of *n*-BuLi (2.5 M，4.33 mL，10.85 mmol). After the addition, the mixture was kept at 0 °C and stirred for 3 h. For the other reaction, cyanuric chloride (1.00 g，5.42 mmol) was dissolved in 9.51 mL of diethyl ether under nitrogen atmosphere and then added into the above solution slowly.

The mixture was stirred at 0 °C for 9 h. Afterward, the precipitate was filtered out and washed with cold diethyl ether to get 1.03 g (45%) of compound **8** as a white solid. ^{1}H NMR (400 MHz, $CDCl_3$) δ = 8.47 (d, *J* = 8.1 Hz, 4H), 7.69 (d, *J* = 8.5 Hz, 4H). ^{13}C NMR (101 MHz, $CDCl_3$) δ = 172.86, 133.26, 132.38, 130.99, 129.15, 1.17. HRMS (FD, [M]) for C15H8N3ClBr2 calcd. 422.8779, found: 422.8789.

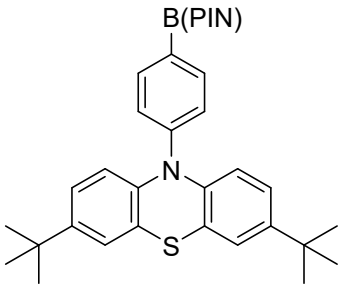

10

1-((4-(3,7-di-tert-butyl-10H-phenothiazin-10-yl)phenyl)-λ²-boraneyl)-1H-1λ³,2,3-iodazaphosphirene, ***10****.* Compound **9** (1.00g, 2.14 mmol), bis(pinacolato)diboron (1.09 g, 4.28 mmol), KOAc (0.63 g, 6.43 mmol) and $Pd(dppf)Cl_2$ (0.08 g, 0.11 mmol) were added into a single-neck round-bottom flask under nitrogen atmosphere, and then 10 mL of 1,4-dioxane was added. The solution was heated to ~110 °C under reflux and stirred for 16 h. After the reaction, 1,4-dioxane was removed by a rotary evaporator and then ethyl acetate was added to extract with brine for three times. After dried by anhydrous $MgSO_4$, the solvent was removed under reduced pressure and the product was purified by column chromatography on silica gel with hexane/ethyl acetate (99:1, v/v) as eluent to get 0.77 g (70%) of compound **10** as a white solid. ^{1}H NMR (400 MHz, $(CD_3)_2CO$) δ = 7.93 (d, *J* = 8.4 Hz, 2H), 7.33 (d, *J* = 8.4 Hz, 2H), 7.17 (d, *J* = 2.3 Hz, 2H), 7.04 (dd, *J* = 8.6, 2.3 Hz, 2H), 6.41 (d, *J* = 8.6 Hz, 2H),1.37 (s, 12H) ,1.26 (s, 18H). ^{13}C NMR (101 MHz, $(CD_3)_2CO$) δ = 147.08, 145.97, 142.12, 137.69, 127.56, 124.82, 123.56, 118.94, 84.70, 34.69, 31.50, 25.22. HRMS (FD, [M]) for C32H40BNO2S calcd. 513.2878, found: 513.2881.

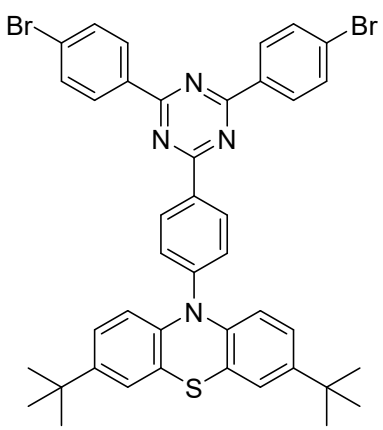

T2

10-(4-(4,6-bis(4-bromophenyl)-1,3,5-triazin-2-yl)phenyl)-3,7-di-tert-butyl-10H-phenothiazine, ***T2****.* Compound **10** (2.41 g, 4.70 mmol), compound **8** (1.00 g, 2.35 mmol), K_2CO_3 (1.30 g, 9.40 mmol), and $Pd(PPh_3)_4$ (0.14 g, 0.12 mmol) were added into a single-neck round-bottom flask under nitrogen atmosphere, followed by the addition of 11.75 mL of dry toluene, 2.03 mL of ethanol, and 2.03 mL of water. The mixture was heated to 75 °C under reflux and stirred for 16 h. Afterward, toluene was removed by a rotary evaporator and then CH_2Cl_2 was added to extract with brine for three times. After dried by anhydrous $MgSO_4$, the solvent was removed under reduced pressure and the product was purified by column chromatography on silica gel with hexane as eluent to get 0.31 g (17%) of compound **T2** as a yellow solid. ^{1}H NMR (400 MHz, $CDCl_3$) δ = 8.67 (d, *J* = 8.8 Hz, 2H), 8.57 (d, *J* = 8.6 Hz, 4H),

7.67 (d, J = 8.5 Hz, 4H), 7.33 (d, J = 8.5 Hz, 4H), 7.19 (d, J = 8.3 Hz, 2H), 6.98 (d, J = 8.4 Hz, 2H), 1.32 (s, 18H). ^{13}C NMR (100 MHz, $CDCl_3$) δ= 170.86, 148.23, 139.99, 135.29, 132.03, 130.94, 130.54, 127.63, 125.24, 124.25, 122.58, 120.93, 34.61, 31.45. HRMS (FD, [M]) for C41H36N4SBr2 calcd. 774.1033, found: 774.1049.

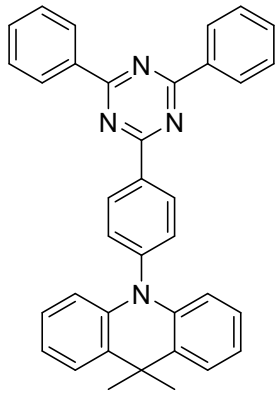

13

10-(4-(4,6-bis(4-bromophenyl)-1,3,5-triazin-2-yl)phenyl)-3,7-di-tert-butyl-10H-phenothiazine10-(4-(4,6-diphenyl-1,3,5-triazin-2-yl)phenyl)-9,9-dimethyl-9,10-dihydroacridine, ***13***.[4] 4-(9,10-dihydro-9,9-dimethylacridine)phenylboronic acid pinacol ester (230 mg, 0.56 mmol), 2-chloro-4,6-diphenyl-1,3,5-triazine (150 mg, 0.56 mmol), Cs_2CO_3 (1.28 g, 3.92 mmol)and $Pd(PPh_3)_4$ (13.0 mg, 0.011 mmol) were added into a flask under nitrogen atmosphere, followed by the addition of 28 mL of dry THF and 7 mL of water. The mixture was heated to 75 °C under reflux and stirred for 16 h. Afterward, THF was removed by a rotary evaporator and then CH_2Cl_2 was added to extract with brine for three times. After dried by anhydrous $MgSO_4$, the solvent was removed under reduced pressure to get the crude product for the next bromination.

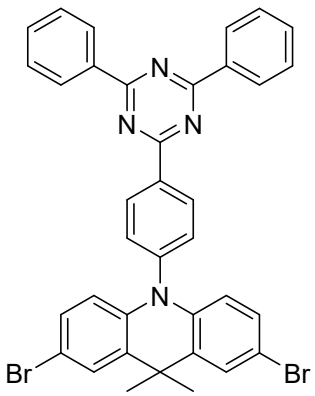

T4

2,7-dibromo-10-(4-(4,6-diphenyl-1,3,5-triazin-2-yl)phenyl)-9,9-dimethyl-9,10-dihydroacridine, ***T4***.[4] Compound **13** (250 mg, 0.48 mmol) was dissolved in 19 mL of dry DMF in a flask under nitrogen atmosphere. *N*-bromosuccinimide (180 mg, 1.03 mmol) was then added and the mixture was stirred at room temperature for 15 h. Afterward, methanol was added to stop the reaction and the precipitate was then collected. The residue was further rinsed with copious methanol. The solvent was removed under reduced pressure and the product was purified by column chromatography on silica gel with hexane/ethyl acetate (10:1, v/v) as eluent to get 320 mg (99%) of compound **T4** as a light-yellwo solid. ^{1}H NMR (400 MHz, $CDCl_3$) δ = 9.03 (d, J = 6.8 Hz, 2H), 8.81 (d, J = 6.8 Hz, 2H), 7.62 (dt, J = 12.8, 5.9 Hz, 6H), 7.54 (s, 2H), 7.50 (d, J = 7.4 Hz, 2H), 7.08 (dt, J = 8.9, 1.9 Hz, 2H), 6.24 (d, J = 8.9 Hz, 2H), 1.68 (s, 6H).

General Procedures of Polymerization. For the synthesis of conjugated polymers, we employed Stille coupling as displayed in Figure 2. Briefly, compound BDT (0.016 mmol), compound SBO (0.011 mmol), compound T1/T2/T3/T4 (0.005 mmol) and $Pd(PPh_3)_4$ (1.44 mg) were used in the polymerization crossing-coupling in dry toluene for 12 h at 90-100 °C. After the polymerization, the

products were purified by reprecipitation in cold methanol/acetone and washed with copious cold acetone/methanol. The products were dissolved in CH_2Cl_2 to extract with brine for three times to obtain 10-15 mg of polymers.

	BDT-SBO	BDT-SBOT1	BDT-SBOT2	BDT-SBOT3	BDT-SBOT4
M_n	81021	58620	105079	20199	115666
M_w	97261	67911	124494	34667	136087
PDI	1.20	1.16	1.18	1.72	1.18

*Preparation of **IR-Pttc/IR-TPE/IR-TPA** Pdots.* Typically, 200 μL of semiconducting polymer BDT-SBO or BDT-SBOT1 or BDT-SBOT2 or BDT-SBOT3 or BDT-SBOT4 solution (1 mg/mL in THF), 80 μL of mPEG-DSPE, and 80 μL of DOPG (1 mg/mL in THF) were mixed well in 5 mL THF. The THF solutions containing polymers were injected into 10 mL H_2O under vigorous sonication. After that, THF was removed under reduced pressure at room temperature. The resulting Pdot solution was passed through a 0.2 μm cellulose acetate syringe filter and were ready for use. The as-prepared Pdot solution was optically stable for at least two weeks at room temperature in the dark.

Characterization of Pdots. The average particle size/zeta potential was determined by dynamic light scattering and transmission electron microscopy (TEM). TEM images of the synthesized Pdots were acquired using a JEOL 2100 transmission electron microscope at an acceleration voltage of 200 kV. For TEM, a drop of Pdot aqueous solution was placed onto a carbon-coated grid and allowed to evaporate at room temperature. The absorption spectra of Pdots were measured using UV-visible spectroscopy (Dynamica Halo DB20S, Dynamica Scientific or Sol 1.7, B&W Tek). The fluorescence spectra were collected using a FS5 spectrofluorometer (Edinburgh Instruments Ltd, UK) under 827 nm excitation.

Determination of Fluorescence Quantum Yields. The fluorescence quantum yields (QY) of the polymers or monomers were determined from the relative fluorescence quantum yields by comparing with the IR-1061 dye (QY = 1.70 % in CH_2Cl_2) as the reference.[5] The equation used was as follows:

$$QY_s = QY_r \times (K_s/K_r) \times (n_s/n_r)^2$$

Where subscripts s and r denote sample and reference, respectively. *K* is the slope of the integrated fluorescence intensity against the absorbance plot (linear fitting for at least five points). *n* is the refractive index of the solvent. The maximal absorptions of all samples were carefully controlled to lower than 0.1 for all measurements to eliminate self-quenching or re-absorption/re-emission issues. The optical parameters used for the measurements were as follows: BDT-SBO/BDT-SBOT1/BDT-SBOT2/BDT-SBOT3/BDT-SBOT4 Pdots vs. IR-1026 (λ_{ex} = 793 nm, λ_{em} =950-1400 nm).

MTT Assay. The cellular cytotoxicity of the Pdots was examined on HeLa cells. The number of viable cells was determined using the MTT assay with 3-(4,5-dimethylthiazole-2-yl)-2,5-phenyltetrazolium bromide. HeLa cells were first seeded in each well of a 24-well culture plate and then incubated with various concentrations of Pdots (5 μg/mL, 10 μg/mL, and 20 μg/mL) for 6 h, 12 h, and 24 h. After that, 20 μL (5 mg/mL) of MTT aqueous solution was added to each well and the cells were further incubated for 4 h at 37 °C to deoxidize MTT. The medium was then washed out and 300 μL of DMSO was added into each well to dissolve formazam crystals. Absorbance was measured by a BioTek ELx800 microplate reader at 570 nm, while the cells cultured with the pure medium (e.g., without Pdots) served as controls.

Density Functional Theory Calculation.

DFT-calculations were carried out at the theory level of B3LYP-D3/6-31G(d) to obtain all optimized structures and frequency analyses of the ground states. We carefully optimize the structures of these oligomer model molecules with dihedral angles between neighboring moieties varied. The acceptor structure (A, SBO, Figure S4), the S of two thiophene group and 1,2,3-triazole are both in opposite positions, which is the most stable structure. However, the free energy difference among different conformers is less than 0.9 kcal/mol (0.88 kcal/mol, 298 K). Moreover, the S atom of the donor (D (BDT), the blue in Figure S4) and the S atom of thiophene group are preferred in a opposite position. The most stable configuration and optimized structures of D-A and D-A-D as shown in Figure S4 and Figure S5. On this basis, we attached TADF moieties, and searched for the lowest energy structure. The time-dependent DFT with the Tamm-Dancoff approximation[6] (TDDFT-TDA) was calculated at the CAM-B3LYP/6-31G(d) level and was obtained the excitation information. Conductor-like polarizable continuum model (CPCM) setting[7-8] for solvent was also employed in our single point energy TDDFT-TDA calculations. The monomeric model molecules were calculated with THF solvent setting. Since the dimers were employed to simulate the optical properties of Pdots, we employ a dielectric parameter for *n*-$C_{15}H_{32}$ for CPCM calculation for both the structural optimization and excitation, as they are surrounded by the nonpolar side of mPEG-DSPE. All the DFT calculations were carried out employing Gaussian 16 Revision A.03.[9] In all calculation, all the alkyl groups are replaced by methyl groups for better computational efficiency.

Fragmented models we adopted to simulate the optical properties of the **BDT-SBOTn** copolymers includes Tn-D-A, D-Tn-D-A, A-D-Tn-D-A and Tn-D-A-D. We list their basic properties in Table S2. From these results, it is seen that the molecular properties of D-Tn-D-A and A-D-Tn-D-A are similar to that of Tn-D-A. TADF has little effect on the molecular orbital energies, as seen in

very similar HOMO or LUMO energies for T-D-A vs. D-A. As seen in Figure S6, where we took T4 as an example, the energies of HOMO and LUMO of various combinations of T4, D-A and D-A-D indicate a large discrepancy in the HOMO and LUMO energies of TADF with those of D-A.

Excitation of short oligomers in THF

We first calculate the excitation properties for possible units that can give rise the absorption and emission in the polymer. The calculated HOMO-LUMO gap and absorption wavelengths are listed in Table 2. In Figure S7 we depict the energies of HOMO and LUMO of D-A, among various fragments Tn-D-A, D-A-D and Tn-D-A-D. We have also included the HOMO, LUMO, as well as the natural transition orbitals (NTO)[10] for their S_1 state in Figure 4, S8-9.

The HOMO of D-A is fully delocalized to both D and A fragments, and the LUMO is concentrated in the A moiety. Adding D moiety to A has a significant effect of reducing the HOMO-LUMO gap and a red shift of excitation energy and be seen. Adding TADF moieties does not change the active MOs much. In Tn-D-A models, LUMO is concentrated in the A moiety, while HOMO is delocalized in both D and A. The absorption wavelength is also quite similar to that of D-A. The inactive role of TADF moieties can be understood from their much lower HOMO and much higher LUMO relative to those for D and A, as seen in Figure S6 and Table S2 in the supporting information. For better understanding in the electronic structure, we further simply the dimer system by replacing the TADF group with a methyl group, followed by a partial optimization with only the structure of methyl group and keeping the rest of the system fixed (denoted as Me_{Tn}-D-A). The results are in Table S5. It is seen that the stacking arises from steric effect of TADF is the main cause of spectral change.

In Vivo Fluorescence Blood Vasculature Imaging and 3D Tumor Mapping in Mice with Pdots.

Animal procedures were approved by the Institutional Animal Care and Use Committee (IACUC #1100509) of NYCU. Five-week-old female nude mice (BALB/ cAnN.Cg-Foxn1nu/CrlNarl) were purchased from National Laboratory Animal Center and housed under specific pathogen-free conditions. The facility was maintained at 24 °C with a 12 h light/12 h dark cycle. Before vessel imaging, all mice were anesthetized using a rodent ventilator with air mixed with 2% isoflurane. All groups within the study contained n = 5 mice. The mice were injected with 200 μL of Pdots (5 mg/mL) *via* intravenous injection through the tail

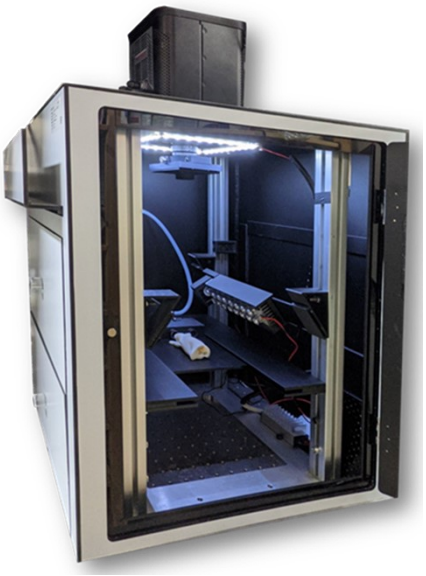

vein. In vivo fluorescence imaging was performed and monitored at the different duration of time of post-injection and then analyzed using a home-built NIR-II imaging instrument with an InGaAs camera (NIRvana 640, Princeton Instruments) by using 793 nm laser (CNI FC-W-793) excitation equipped with a 1200-nm emission long-pass filter (Thorlabs). The InGaAs camera was cooled to -80 °C, the analog to digital conversion rate set to 10 MHz, the gain set to high, and exposure time set to 800 ms. The power density of the excitation laser was 50 mW/cm^2.

The in vivo 3D tumor mapping was performed at six hours post-injection. The nude mice were anesthetized with isoflurane and placed on a homemade rotation system. The excitation power of the laser was 50 mW/cm^2. We took a sequence of fluorescence blood vasculature images at different rotation angles from -45° to 45° with an exposure time of 800 ms. The multi-angle fluorescence images were imported into 3DF Zephyr free software (3DFlow, Verona, Italy) and a dense point cloud was reconstructed from them. The reconstructed 3D tumor images in the XY plane matched well with 2D images.

Supplementary Figures

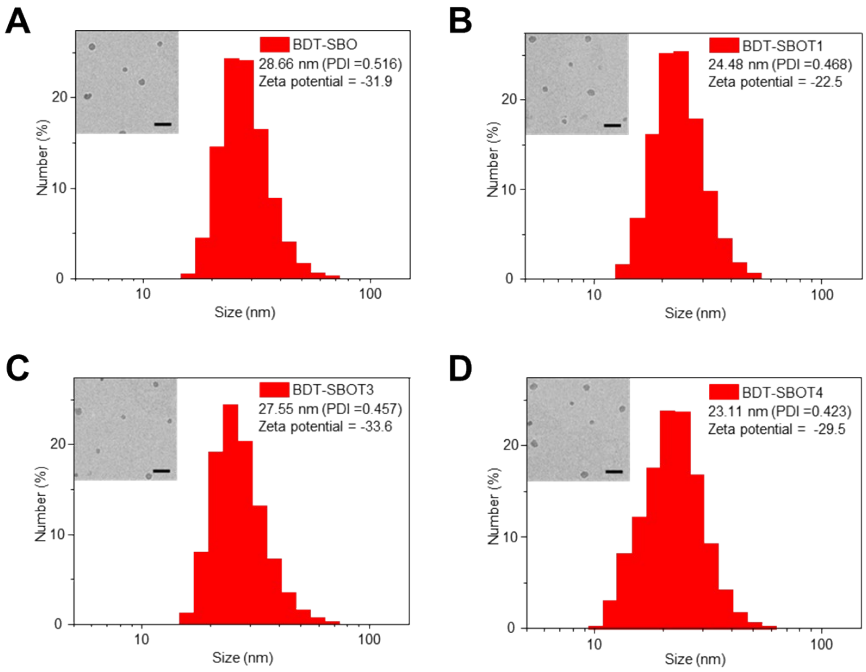

Figure S1. Hydrodynamic diameters of (A) BDT-SBO, (B) BDT-SBOT1, (C) BDT-SBOT3, and (C) BDT-SBOT4 Pdots. The insets on the images represent their corresponding TEM images. The scale bars are 100 nm. The average sizes of the Pdots were 29 nm, 24 nm, 28 nm, and 23 nm for BDT-SBO, BDT-SBOT1, BDT-SBOT3, and BDT-SBOT4 Pdots, respectively. The zeta potentials were determined to be -32 mV, -23 mV, -34 mV, and -30 mV for BDT-SBO, BDT-SBOT1, BDT-SBOT3, and BDT-SBOT4 Pdots, respectively.

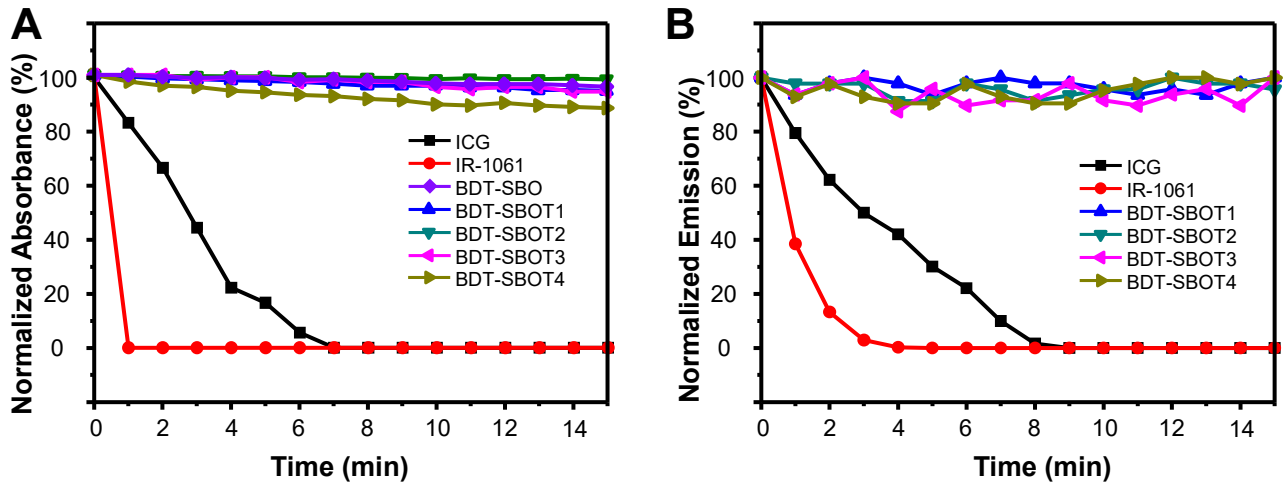

Figure S2. Photostability of several fluorescent probes. (A) Normalized absorption and (B) fluorescence intensity vs. irradiation time of ICG dyes in water (black line), IR-1061 dyes in CH_2Cl_2 (red line), BDT-SBOT Pdots in water (purple line), BDT-SBOT1 Pdots in water (blue line), BDT-SBOT2 Pdots in water (green line), BDT-SBOT3 Pdots in water (pink line), and BDT-SBOT4 Pdots in water (olive green line) under continuous 254 nm UV irradiation. The concentration used for all probe was 0.01 mg/mL in the photostability measurements. Note that the fluorescence intensity of BDT-SBOT Pdots is undetectable due to their low fluorescence QY.

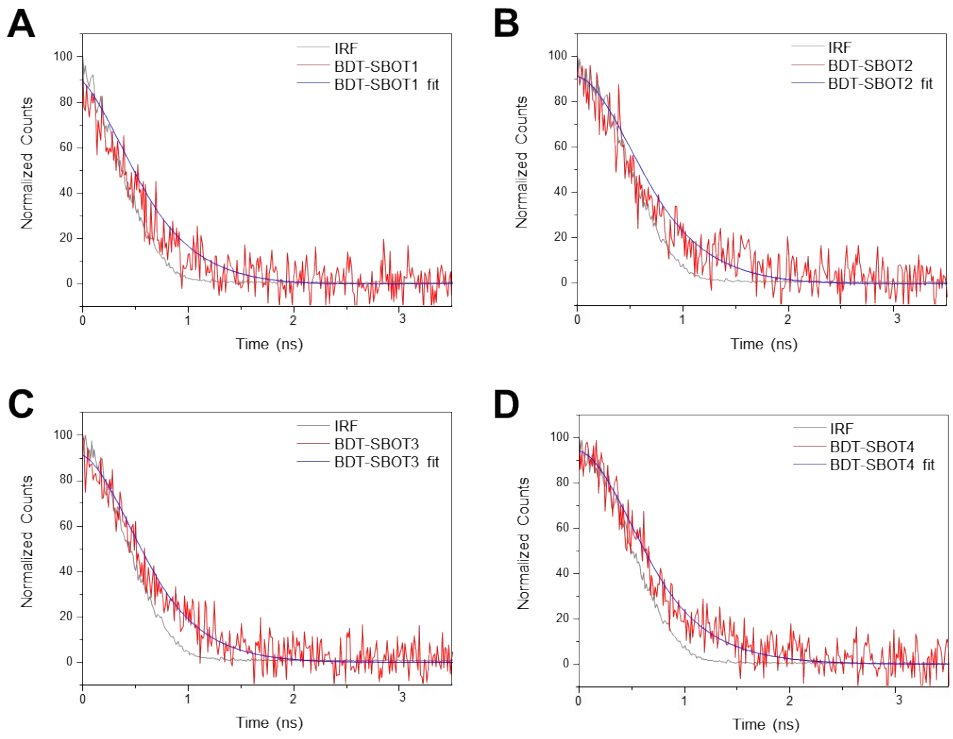

Figure S3. Fluorescence decay lifetime (~3.5 ns) of (A) BDT-SBOT1, (B) BDT-SBOT2, (C) BDT-SBOT3, and (D) BDT-SBOT4 Pdots measured by a time-correlated single-photon counting instrument. The black line represents experimental data and the red line depicts the decay curve fitted with a double exponential decay function. The gray lines show instrument response function.

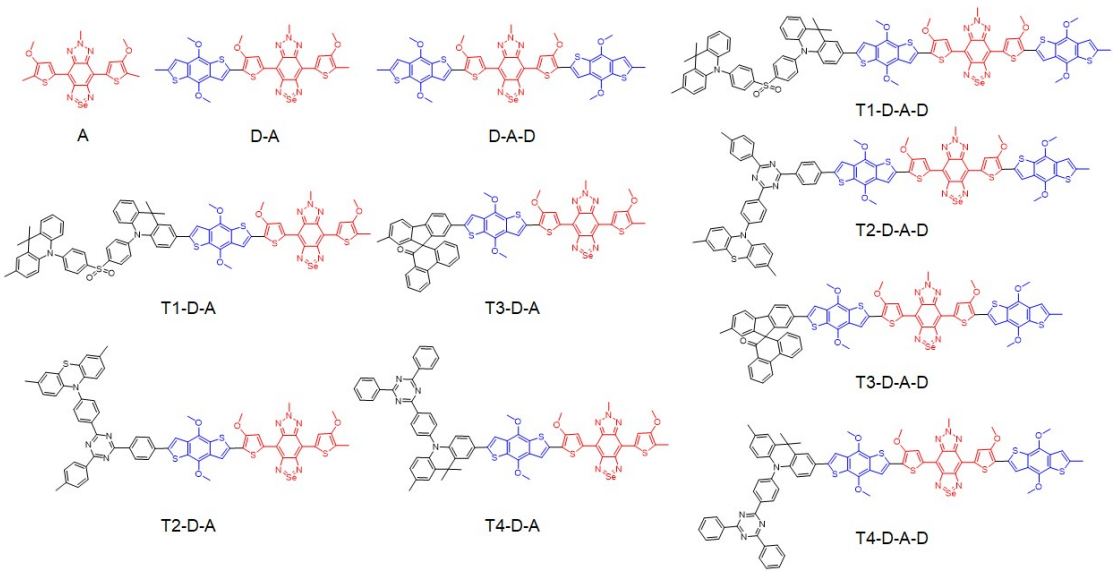

Figure S4. The representative fragmented structures of polymer, the donor group (D, BDT) in blue, the accepter group (A, SBO) in red and the TADF group (T) in black.

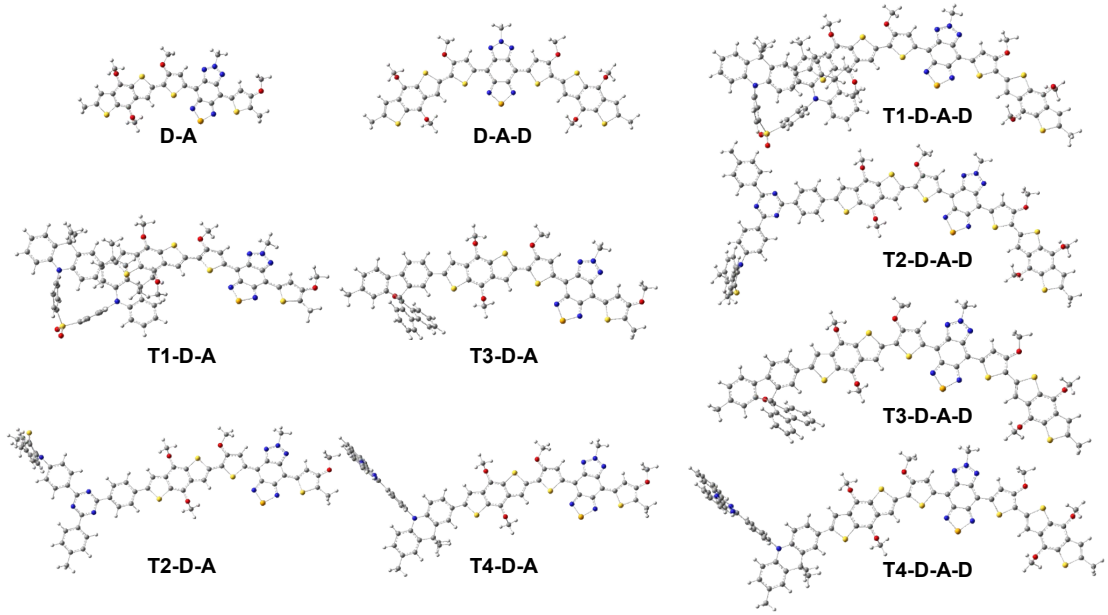

Figure S5. The minimum-energy structures of the fragmented structures after optimization at B3LYP-D3/6-31G(d) level.

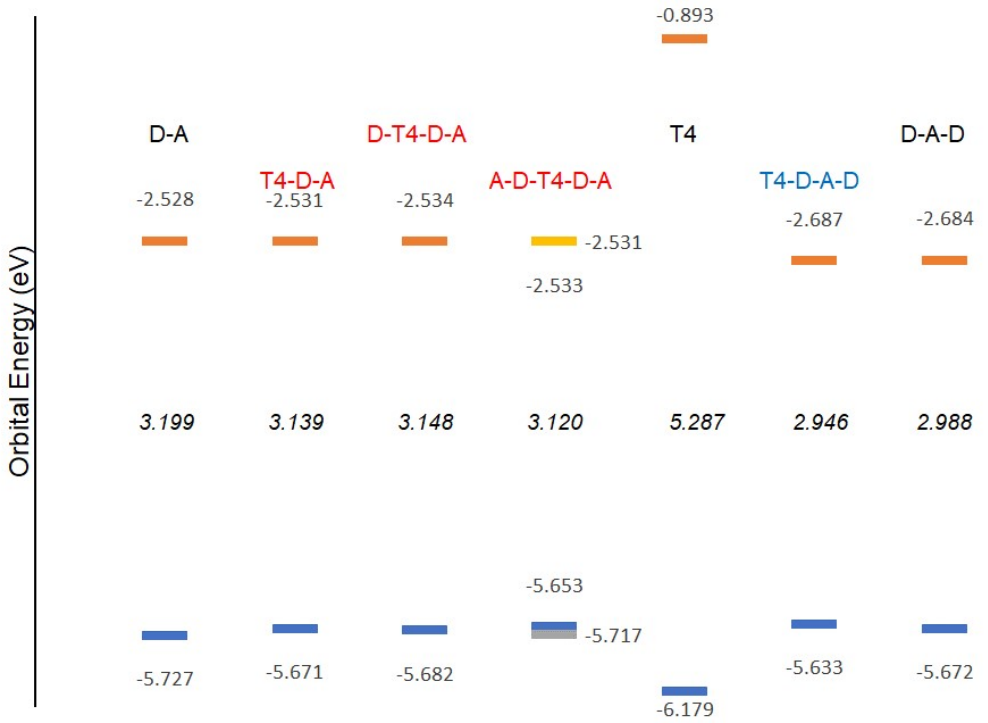

Figure S6. The energy of HOMO, LUMO and HOMO-LUMO energy gap of D-A、T4-D-A、D-T4-D-A、A-D-T4-D-A、T4、T4-D-A-D and D-A-D at the CAM-B3LYP(THF, CPCM)/6-31G(d)//B3LYP/6-31G(d) level.

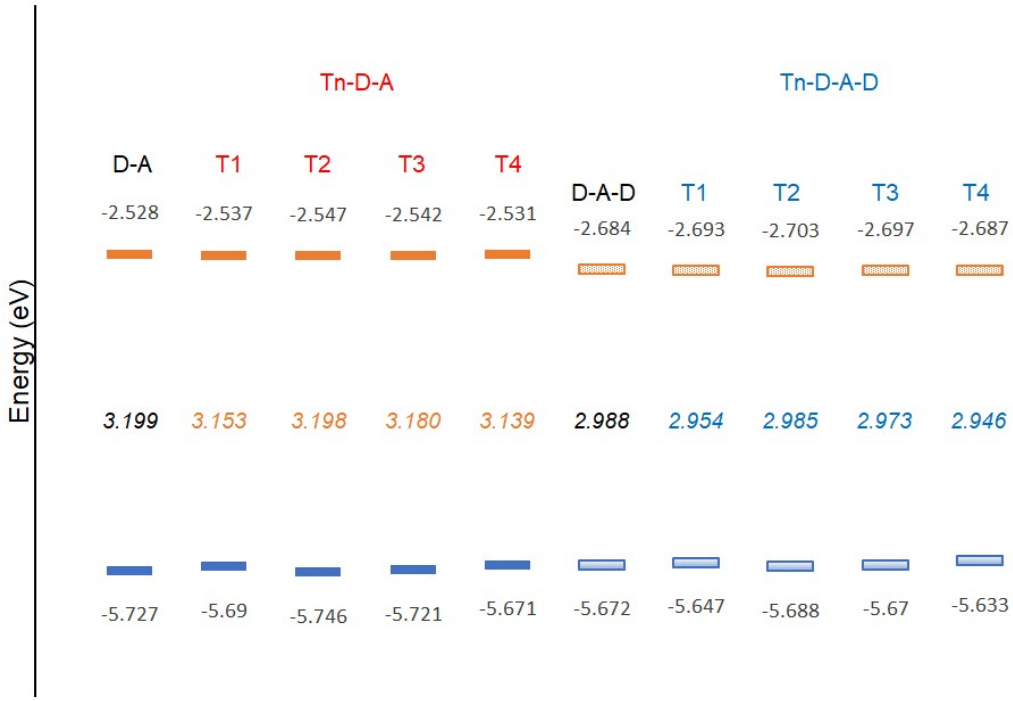

Figure S7. The energy of HOMO (in blue) and LUMO (in orange) and corresponding HOMO–LUMO energy gaps at the CAM-B3LYP(THF, CPCM)/6-31G(d)//B3LYP-D3/6-31G(d) level.

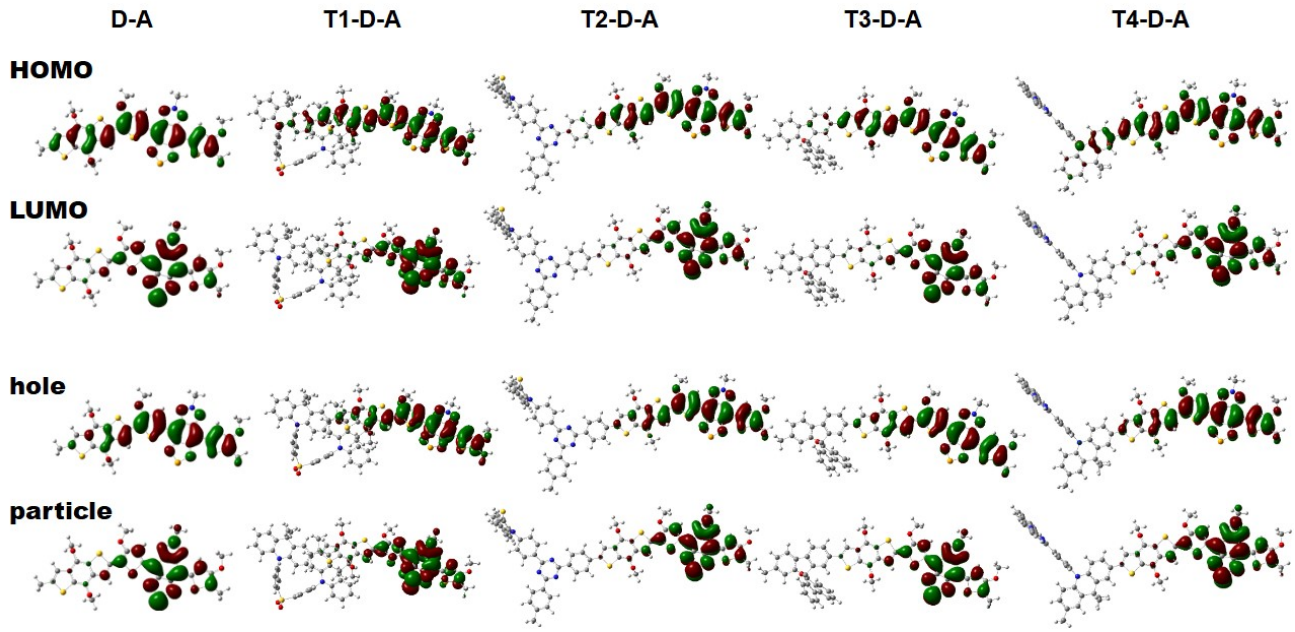

Figure S8. The electron density contours of HOMO, LUMO, computed natural transition orbital (NTO) pairs for S1 of D-A, T1-D-A, T2-D-A, T3-D-A and T4-D-A based on DFT calculations. The isosurface value was set at 0.02 a.u.

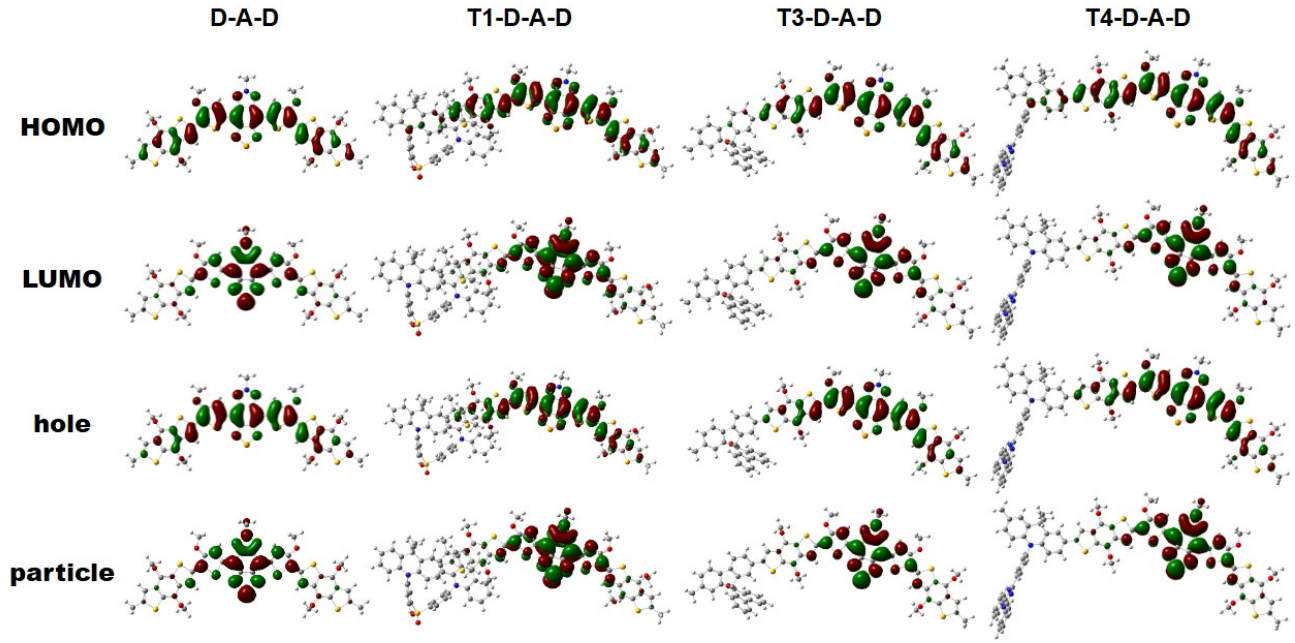

Figure S9. The electron density contours of HOMO, LUMO, computed natural transition orbital (NTO) pairs for S1 of D-A-D, T1-D-A-D, T3-D-A-D and T4-D-A-D based on DFT calculations. The isosurface value was set at 0.02 a.u.

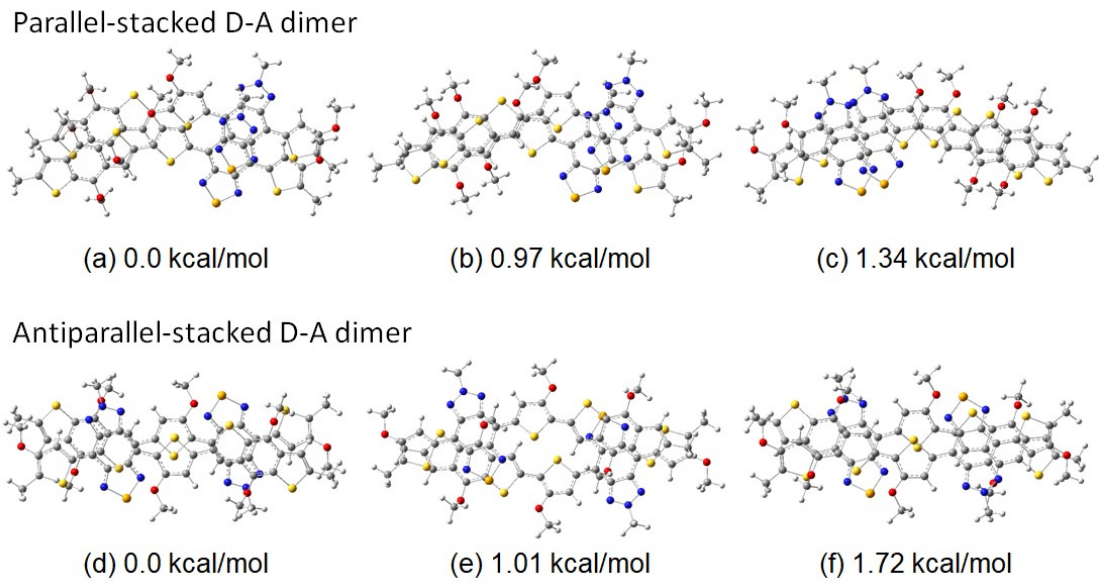

Figure S10. The optimized structure at B3LYP-D3/6-31G(d) level of (a)-(c) the parallel-stacked and (d)-(f) antiparallel stacked D-A dimer. The energy here is the relative energy relative to the most stable parallel stack or antiparallel stack dimer at the CAM-B3LYP(*n*-$C_{15}H_{32}$, CPCM)/6-31G(d)//B3LYP-D3/6-31G(d) level.

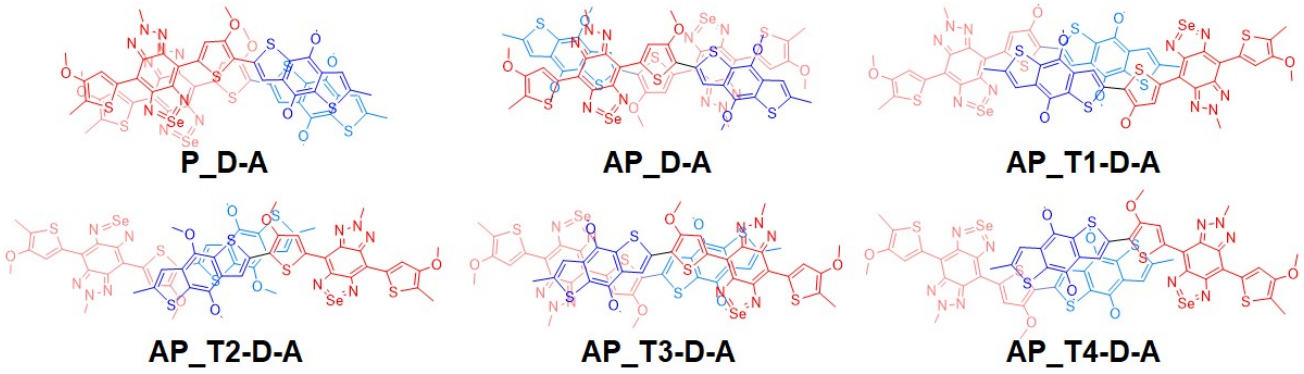

Figure S11. Depicted structures of antiparallel stacked dimer and parallel stacked D-A dimer. TADF moieties were employed in the structural optimization, but for the sake of clarity, they are replaced by a methyl group in this representation. Donor and Accepter are depicted in blue and red respectively, and light colors are used in the lower layer.

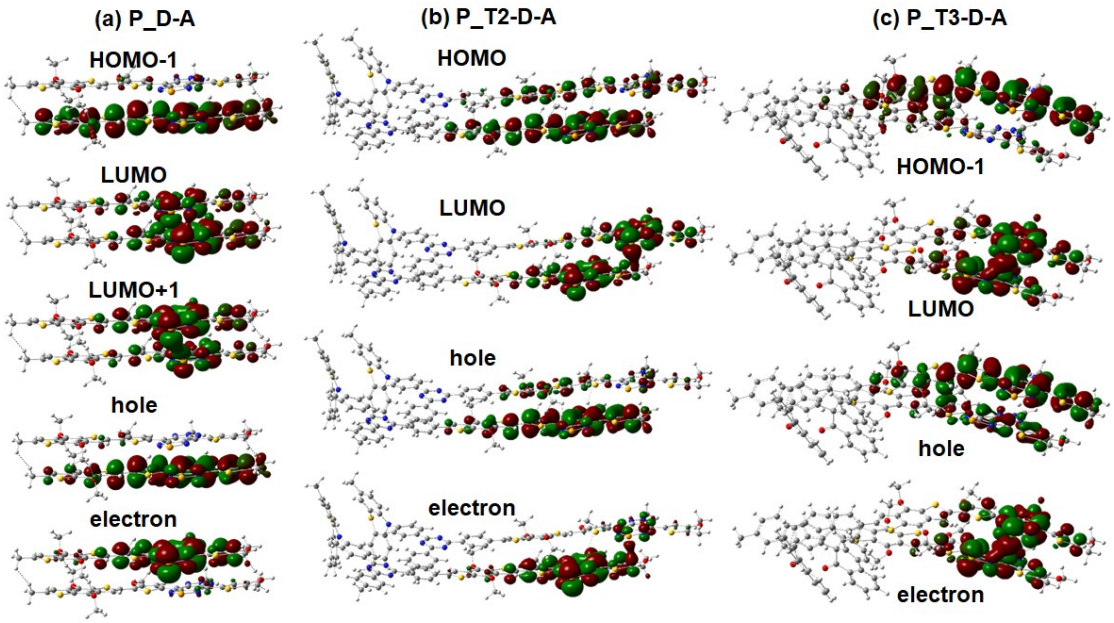

Figure S12. The electron density contours of HOMO, LUMO, computed natural transition orbital (NTO) pairs for (a) S_3 of P_ D-A, (b) S_1 of P_T2-D-A and (c) S2 of P_T3-D-A based on DFT calculations. The isosurfaces were depicted at the value of 0.02 a.u.

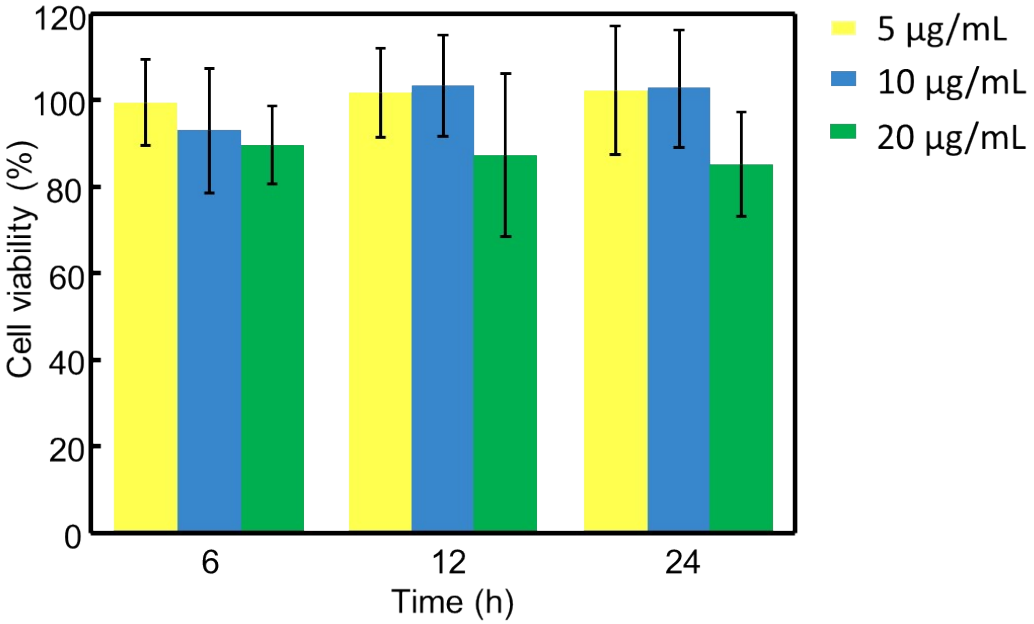

Figure S13. Cytotoxicity results on HeLa cells evaluated by MTT assays. The cells were incubated at different BDT-SBOT2 Pdot concentrations (5-20 μg/mL) at various incubation times (6-24 h).

Table S1. Optical Properties of conjugated polymers in THF under air and inert conditions.

Polymers	λ_{max}^{abs} [nm]	λ_{max}^{emi} [nm]	Stokes shift [nm]	QY air [%]	QY inert [%]
BDT-SBO	835	998	164	2.22	2.24
BDT-SBOT1	822	995	173	2.48	2.68
BDT-SBOT2	821	995	174	5.64	6.77
BDT-SBOT3	827	999	172	3.2	3.58
BDT-SBOT4	830	1004	174	4.3	4.21

Table S2. The orbital energies (eV), HOMO-LUMO gap (E_{gap}, eV), the calculated (λ_{cal}) absorption wavelengths (nm) and oscillator strength (*f*) of D-A type at the level of (TDA)CAM-B3LYP(THF, CPCM)/6-31G(d)//B3LYP-D3/6-31G(d) level.

	HOMO	LUMO	E_{gap}	λ_{cal}	*f*
T1	-6.321	-0.567	5.754	342	0.0161
T2	-6.375	-0.862	5.514	333	0.0006
T3	-7.020	-0.605	6.415	316	0.0146
T4	-6.179	-0.893	5.287	355	0.0000
D(BDT)	-6.624	0.081	6.705	286	0.4625
A(SBO)	-5.815	-2.371	3.444	689	0.7709
D-A	-5.727	-2.528	3.199	743	1.1995
T1-D-A	-5.690	-2.537	3.153	751	1.3176
T2-D-A	-5.746	-2.547	3.198	744	1.3389
T3-D-A	-5.721	-2.542	3.180	747	1.3193
T4-D-A	-5.671	-2.531	3.139	751	1.3314
D-T1-D-A	-5.626	-2.522	3.105	762	1.3336
D-T2-D-A	-5.747	-2.547	3.200	743	1.349
D-T3-D-A	-5.722	-2.543	3.179	747	1.3717
D-T4-D-A	-5.682	-2.534	3.148	750	1.3375
A-D-T1-D-A	-5.612	-2.536	3.075	772	1.5557
	-5.662[a]	-2.514[b]	3.126	747	1.1004
A-D-T2-D-A	-5.743	-2.546	3.197	746	1.2816
	-5.746[a]	-2.545[b]	3.200	741	1.4159
A-D-T3-D-A	-5.697	-2.542	3.155	750	2.6086
	-5.743[a]	-2.536[b]	3.201		
A-D-T4-D-A	-5.653	-2.533	3.120	753	2.5861
	-5.717[a]	-2.531[b]	3.184		
D-A-D	-5.672	-2.684	2.988	814	1.6482
T1-D-A-D	-5.647	-2.693	2.954	823	1.7645
T2-D-A-D	-5.688	-2.703	2.985	816	1.7773
T3-D-A-D	-5.670	-2.697	2.973	819	1.7616
T4-D-A-D	-5.633	-2.687	2.946	824	1.7766
D-A-D-A	-5.496	-2.700	2.795	867	2.7878
T1-D-A-D-A	-5.488	-2.708	2.780	875	2.8656
T2-D-A-D-A	-5.504	-2.718	2.786	871	2.9042
T3-D-A-D-A	-5.498	-2.712	2.785	872	2.8753
T4-D-A-D-A	-5.482	-2.702	2.780	875	2.8720

[a]The energy of HOMO-1. [b]The energy of LUMO+1.

Table S3. The orbital energies (eV) and orbital gap (E_{gap}, eV) in *n*-$C_{15}H_{32}$ solvent of monomer, parallel- and antiparallel dimer at the level of CAM-B3LYP(*n*-$C_{15}H_{32}$, CPCM)//B3LYP-D3 with 6-31G(d) basis sets.

	HOMO	LUMO	HOMO-1	LUMO+1	$E_{gap}{}^{a}$	$E_{gap}{}^{b}$
monomer						
D-A	-5.608	-2.475			3.133	
T1-D-A	-5.593	-2.500			3.093	
T2-D-A	-5.644	-2.511			3.134	
T3-D-A	-5.604	-2.496			3.108	
T4-D-A	-5.536	-2.469			3.066	
Parallel dimer						
D-A	-5.395	-2.452	-5.492	-2.350	2.942	3.045
T1-D-A	-5.467	-2.447	-5.665	-2.374	3.020	3.093
T2-D-A	-5.437	-2.496	-5.685	-2.353	2.941	3.084
T3-D-A	-5.354	-2.534	-5.565	-2.261	2.820	3.092
T4-D-A	-5.302	-2.431	-5.558	-2.283	2.871	3.019
Antiparallel dimer						
D-A	-5.351	-2.258	-5.744	-2.135	3.093	3.216
T1-D-A	-5.442	-2.428	-5.750	-2.386	3.015	3.056
T2-D-A	-5.478	-2.412	-5.668	-2.369	3.066	3.109
T3-D-A	-5.278	-2.410	-5.707	-2.302	2.868	2.976
T4-D-A	-5.437	-2.339	-5.511	-2.290	3.098	3.147
Parallel dimer						
Me_{T1}-D-A	-5.433	-2.391	-5.640	-2.322	3.042	3.111
Me_{T2}-D-A	-5.393	-2.446	-5.637	-2.305	2.947	3.088
Me_{T3}-D-A	-5.346	-2.498	-5.541	-2.225	2.848	3.121
Me_{T4}-D-A	-5.402	-2.450	-5.633	-2.301	2.952	3.101
Antiparallel dimer						
Me_{T1}-D-A	-5.511	-2.429	-5.721	-2.401	3.081	3.110
Me_{T2}-D-A	-5.464	-2.453	-5.594	-2.423	3.010	3.041
Me_{T3}-D-A	-5.307	-2.449	-5.727	-2.336	2.858	2.971
Me_{T4}-D-A	-5.525	-2.442	-5.619	-2.410	3.084	3.116

[a]HOMO-LUMO gap. [b]HOMO-LUMO+1 gap.

Table S4. The HOMO-LUMO gap (E_{gap}, eV), the calculated (λ_{cal}) absorption wavelengths (nm), oscillator strength (f) and occupations (occ.) of NTO pair of model molecules at the level of CAM-B3LYP(n-$C_{15}H_{32}$, CPCM)//B3LYP-D3 with 6-31G(d) basis sets.

	monomer		parallel dimer				antiparallel dimer			
	E_{gap}	λ_{cal}	E_{gap}	λ_{cal}	f	Occ.	E_{gap}	λ_{cal}	f	Occ.
D-A	3.133	768	2.942	895	0.0063	0.92923	3.093	789	1.1601	0.91588
				887[a]	0.0561	0.88792				
				805[b]	0.1716	0.98247				
				728[c]	2.0200					
T1-D-A	3.093	774	3.020	871	0.1711	0.97437	3.015	797	1.7885	0.70216
				843[a]	0.2831	0.90345				
				776[b]	0.1109					
				687[c]	1.6088					
T2-D-A	3.134	767	2.941	854	0.9182	0.93613	3.066	786	2.1045	0.63817
T3-D-A	3.108	772	2.820	975	0.0836	0.97300	2.868	860	1.7891	0.83156
				825[a]	0.2059	0.78540				
				753[b]	0.7187					
				715[c]	1.4608					
T4-D-A	3.066	778	2.871	873	0.8813	0.93514	3.098	770	2.2912	0.66812

[a]The second excited state. [b]The third excited state. [c]The forth excited state.

Table S5. The HOMO-LUMO gap (E_{gap}, eV), the calculated (λ_{cal}) absorption wavelengths (nm) and oscillator strength (f) of model molecules at the level of CAM-B3LYP(n-$C_{15}H_{32}$, CPCM)//B3LYP-D3 with 6-31G(d) basis sets.

	parallel dimer			antiparallel dimer		
	E_{gap}	λ_{cal}	f	E_{gap}	λ_{cal}	f
Me_{T1}-D-A	3.042	869	0.1573	3.081	780	2.1446
		844[a]	0.2464			
Me_{T2}-D-A	2.947	854	0.7691	3.010	802	2.0878
Me_{T3}-D-A	2.848	972	0.0640	2.858	866	1.7753
		826[a]	0.1822			
Me_{T4}-D-A	2.952	854	0.7617	3.084	781	2.2221

[a]The second excited state.

NMR Spectra

^{1}H NMR of compound **3**

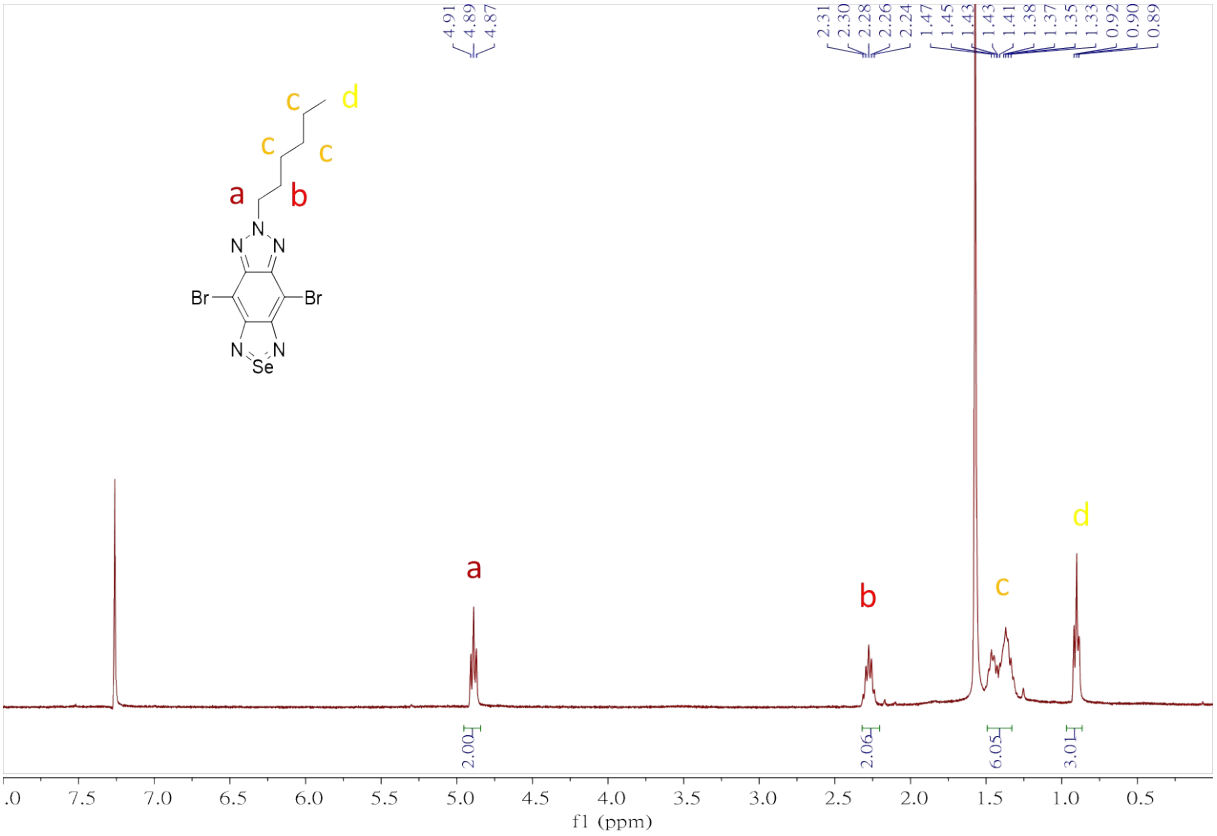

^{13}C NMR of compound **3**

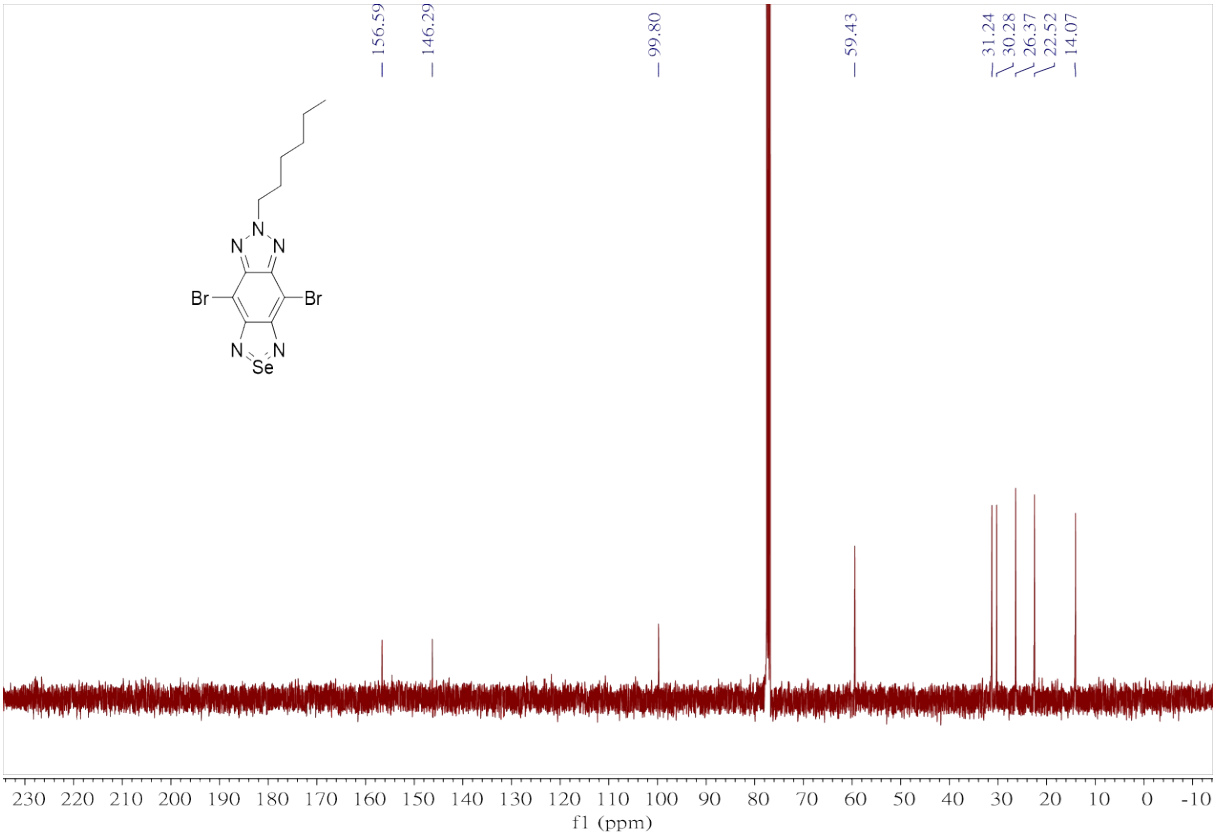

HR-Mass of compound **3**

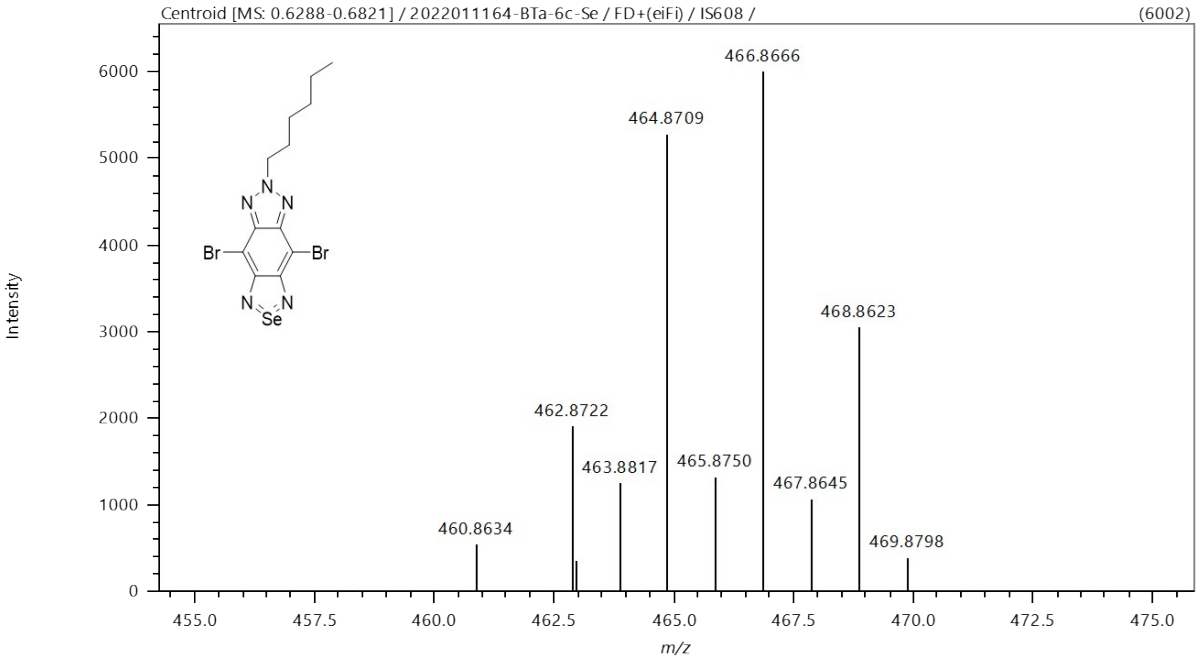

^{1}H NMR of compound **4**

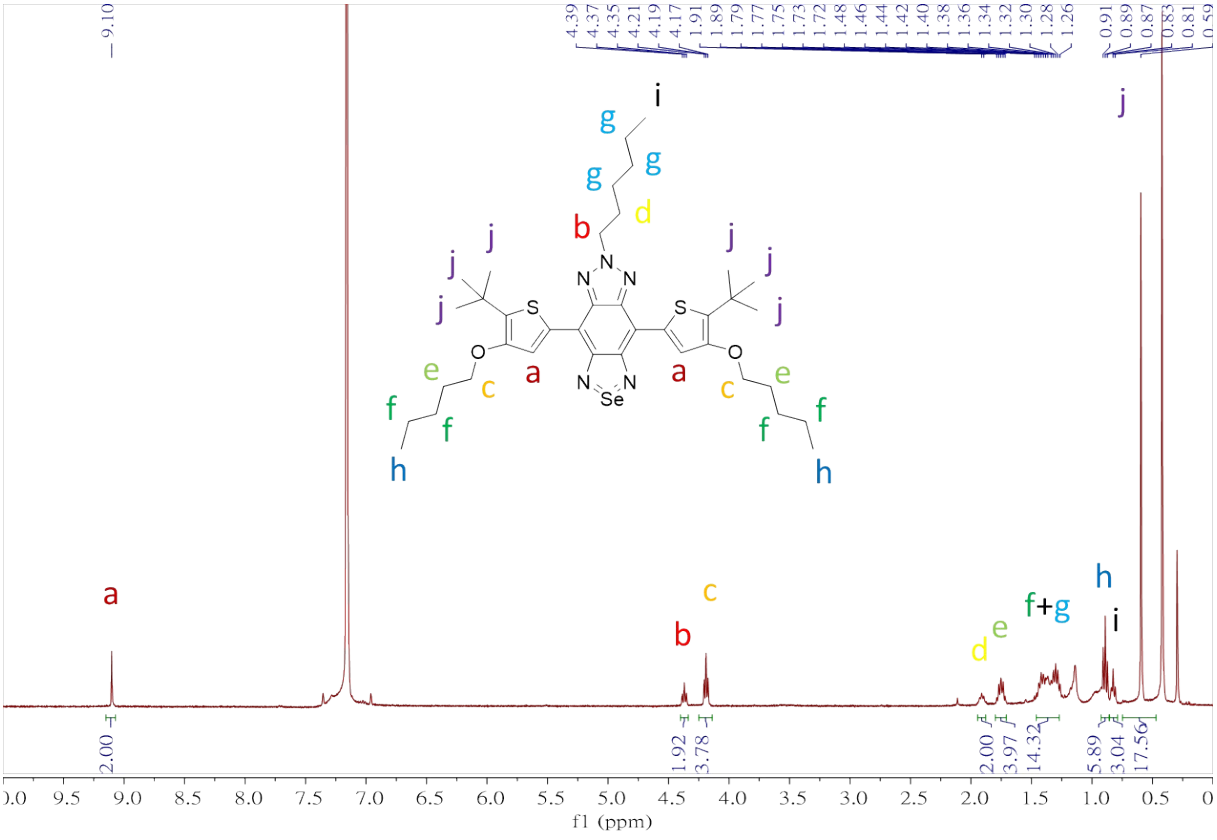

^{13}C NMR of compound **4**

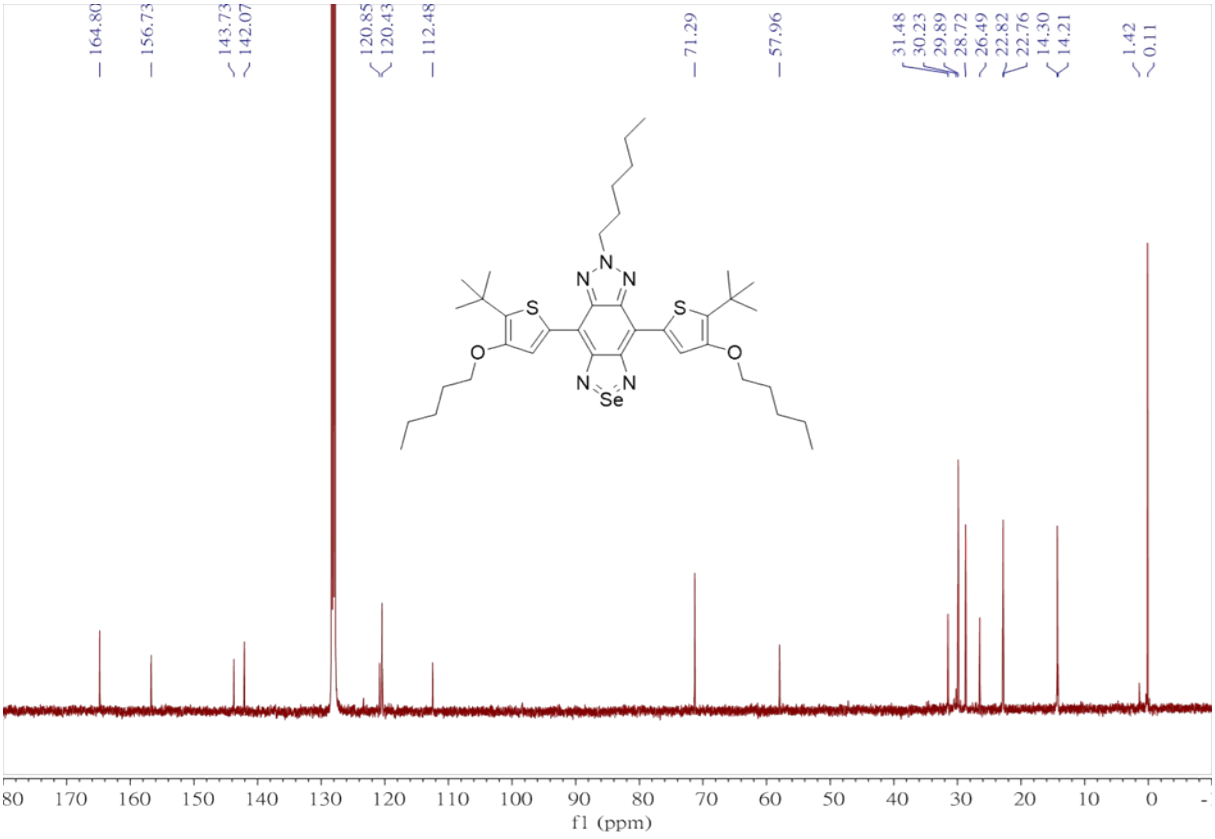

HR-Mass of compound **4**

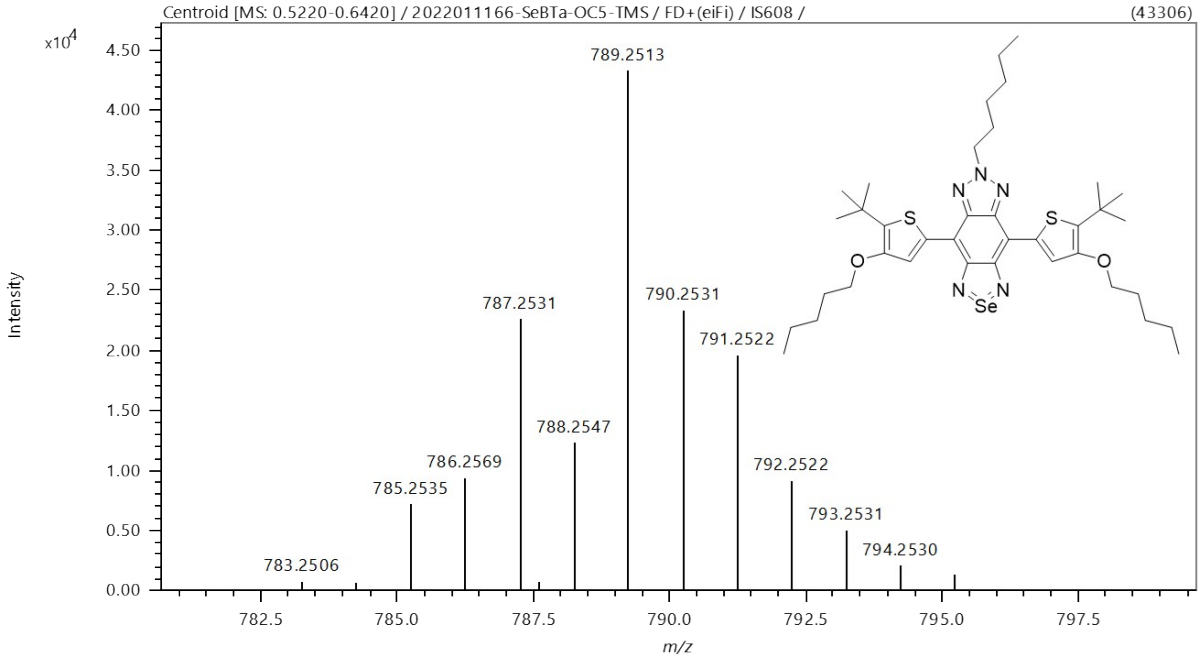

^{1}H NMR of compound **SBO**

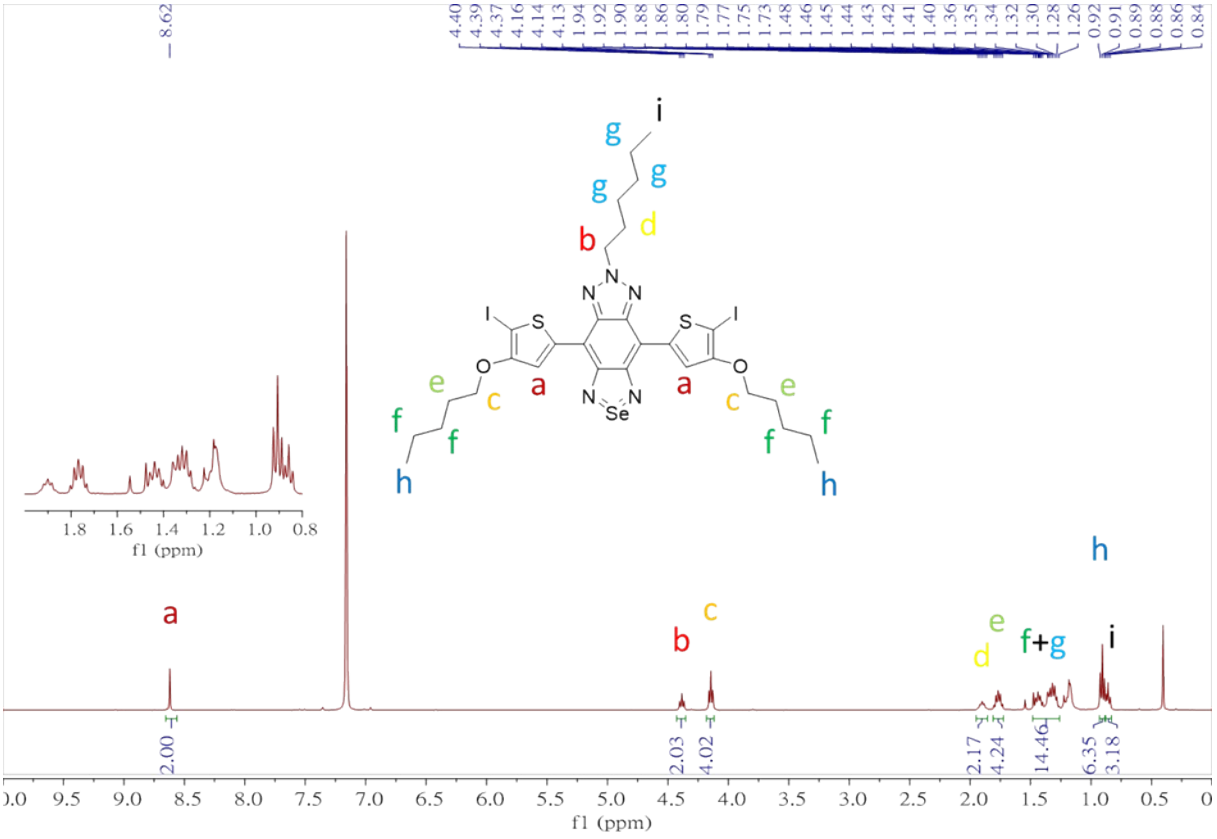

^{13}C NMR of compound **SBO**

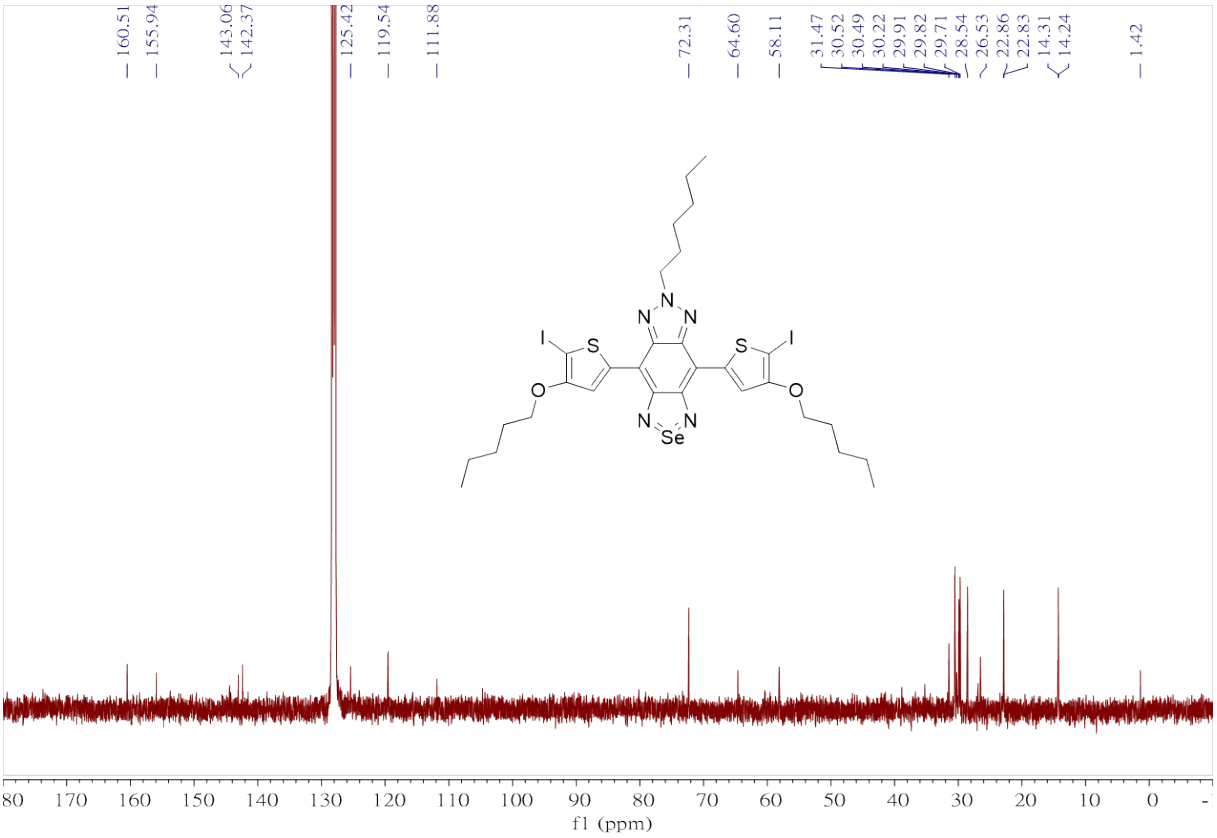

HR-Mass of compound **SBO**

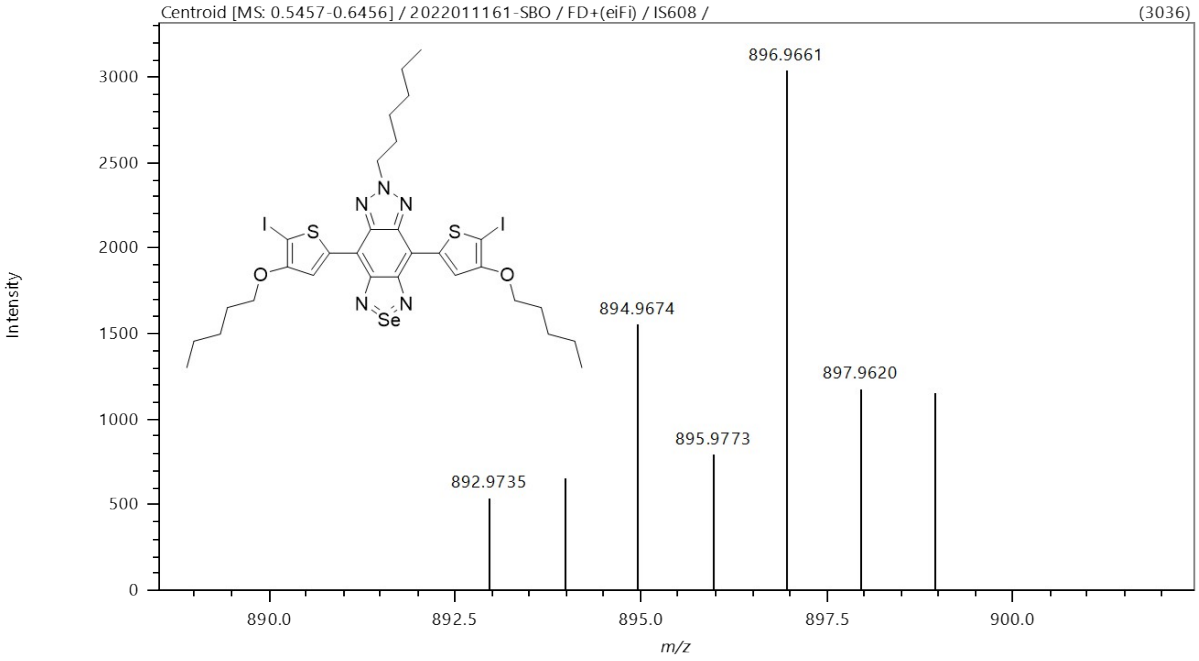

^{1}H NMR of compound **5**

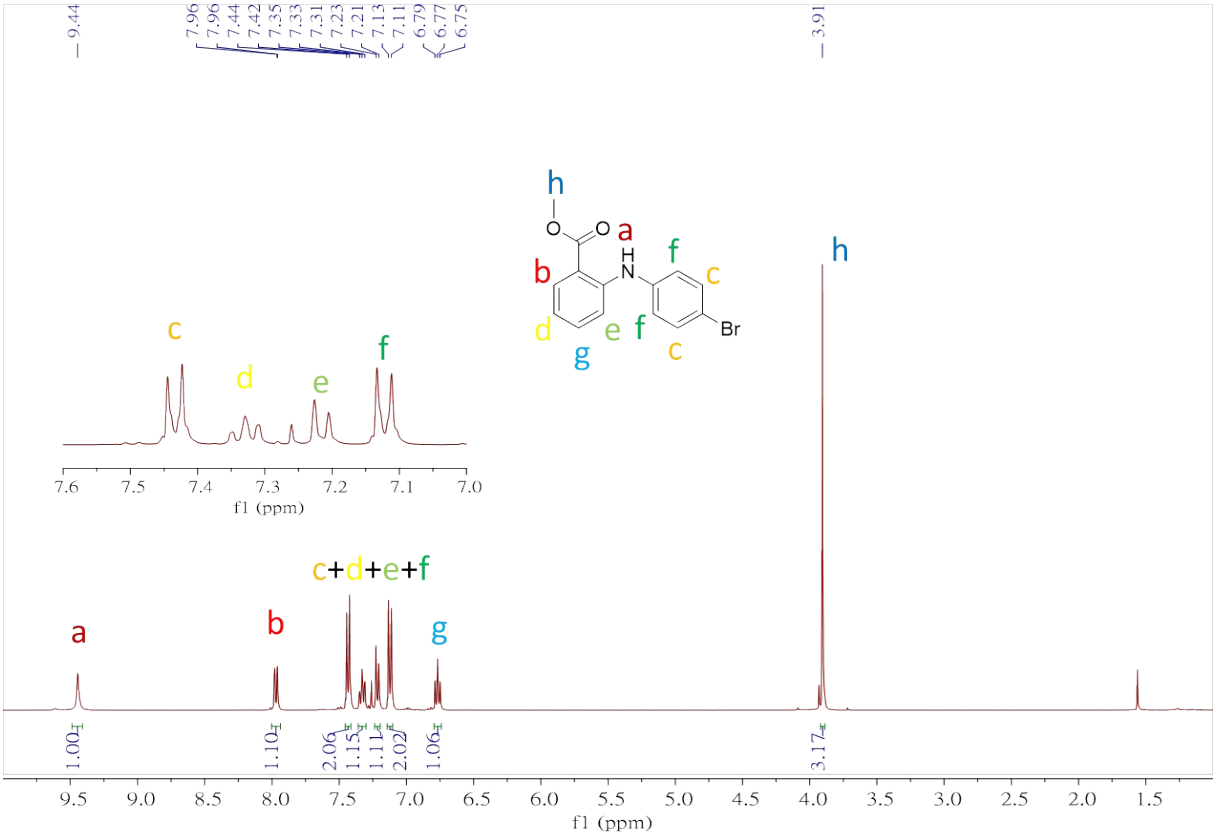

^{13}C NMR of compound **5**

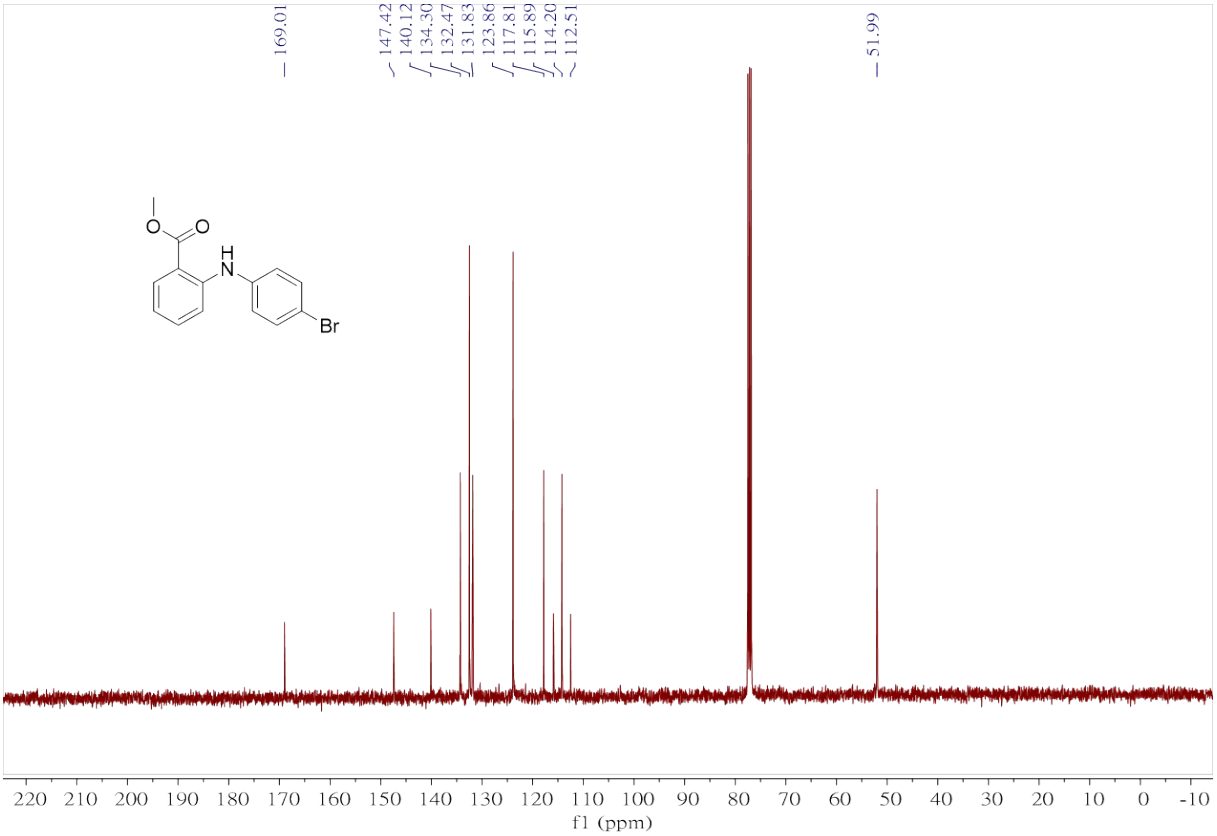

HR-Mass of compound **5**

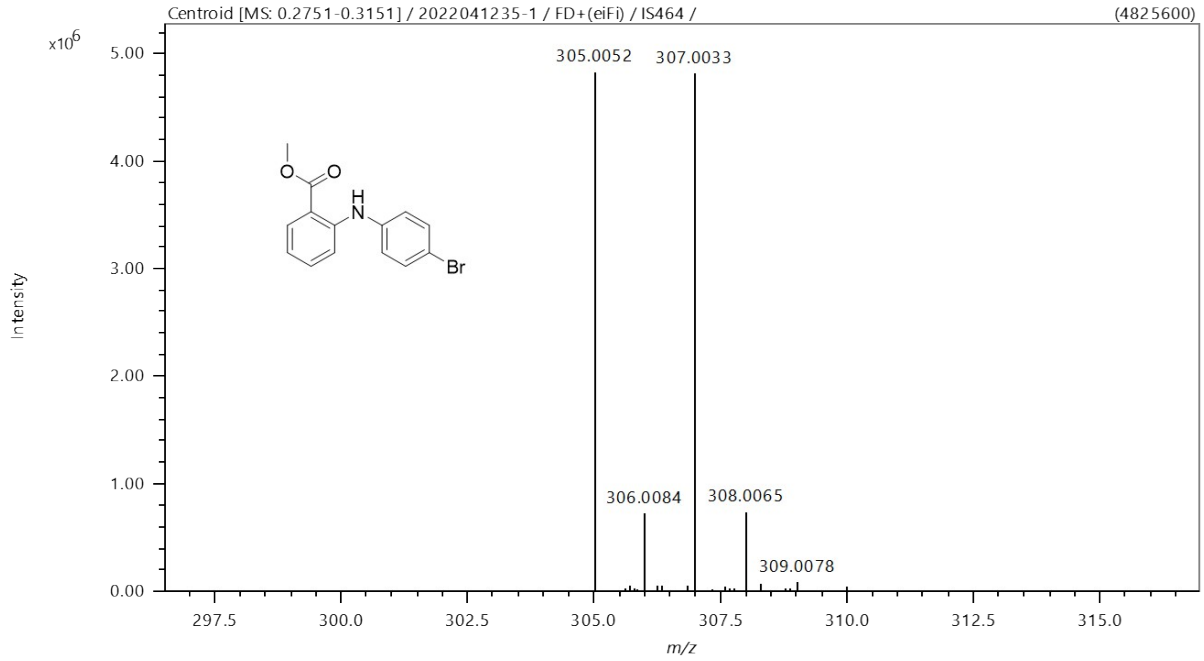

^{1}H NMR of compound **6**

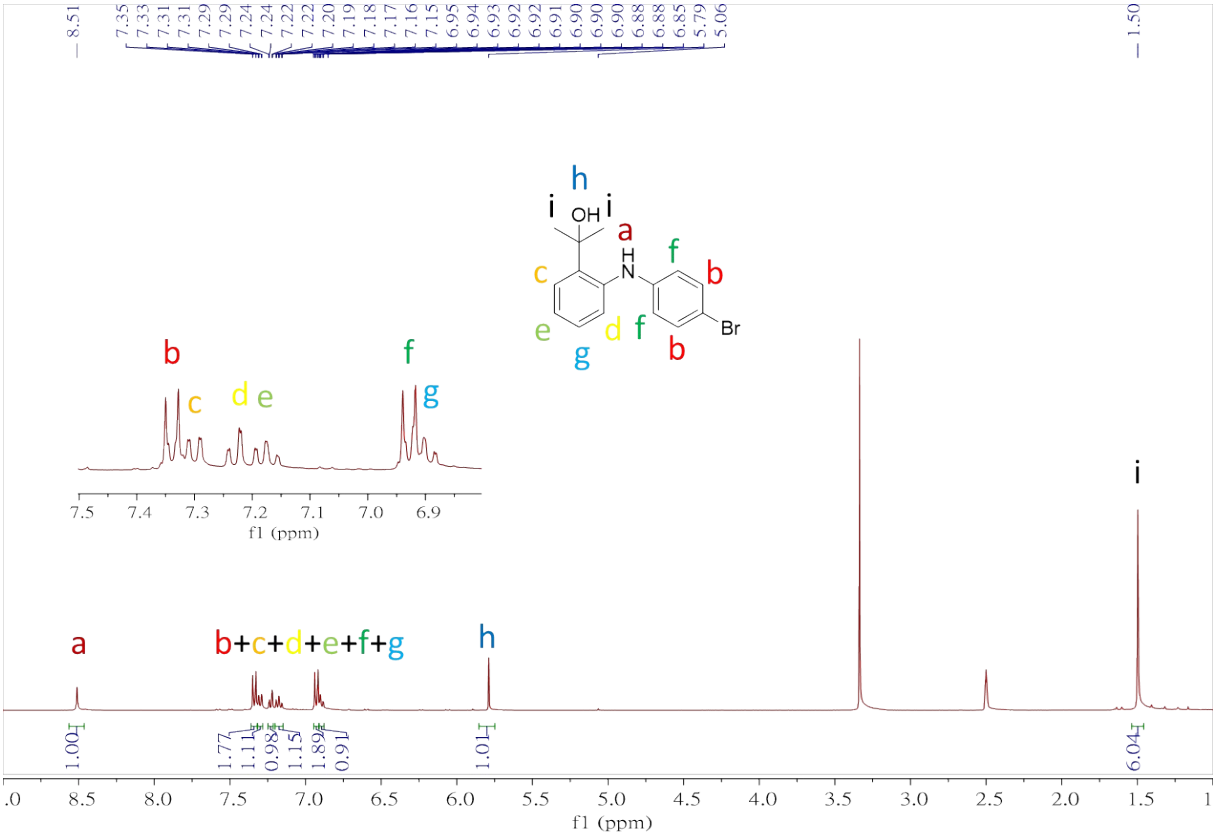

^{13}C NMR of compound **6**

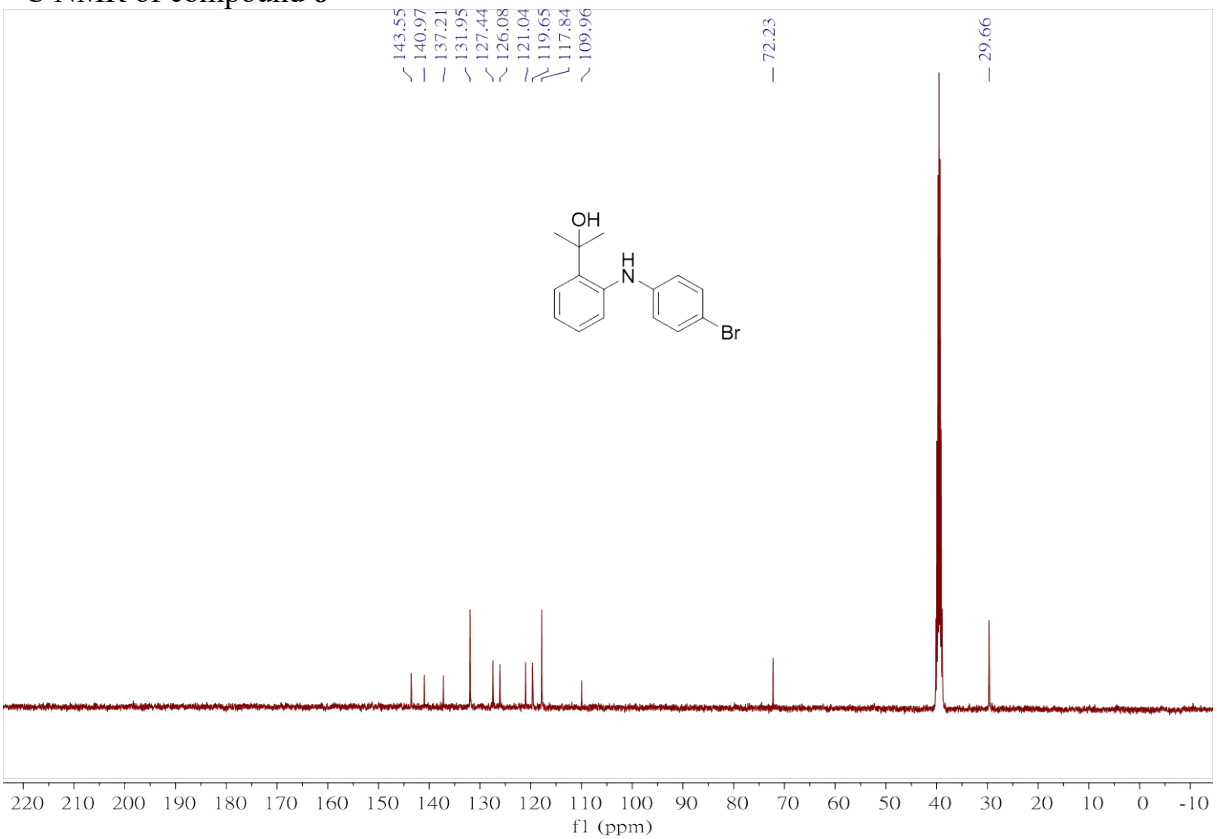

HR-Mass of compound **6**

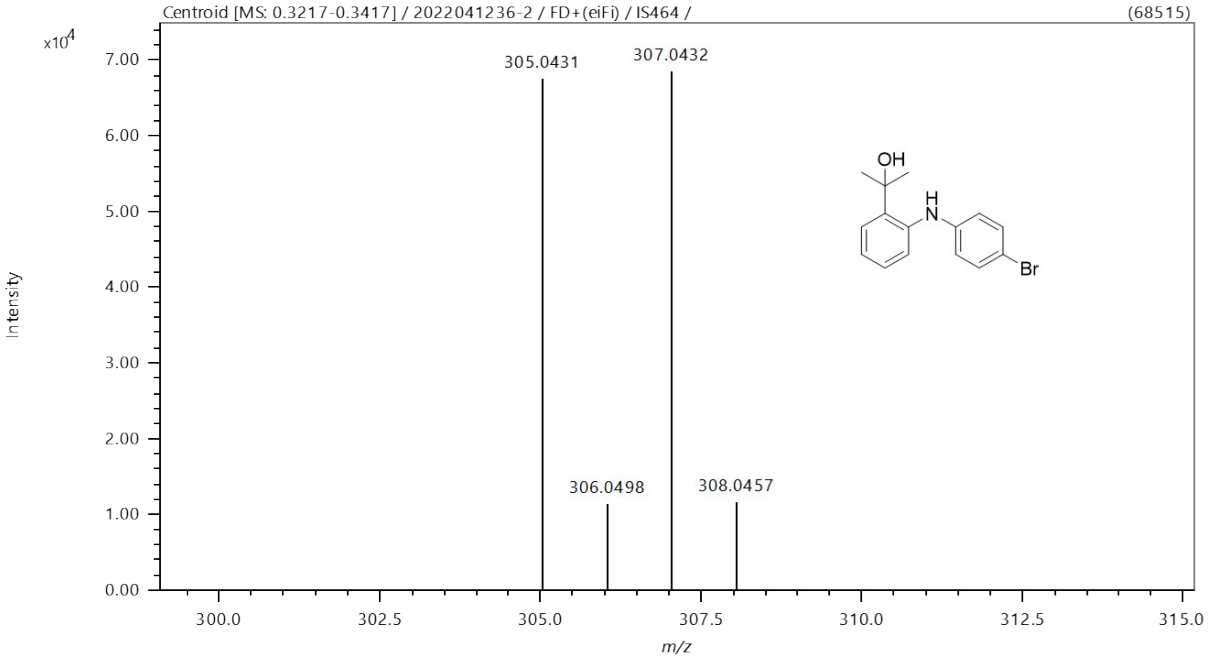

^{1}H NMR of compound **7**

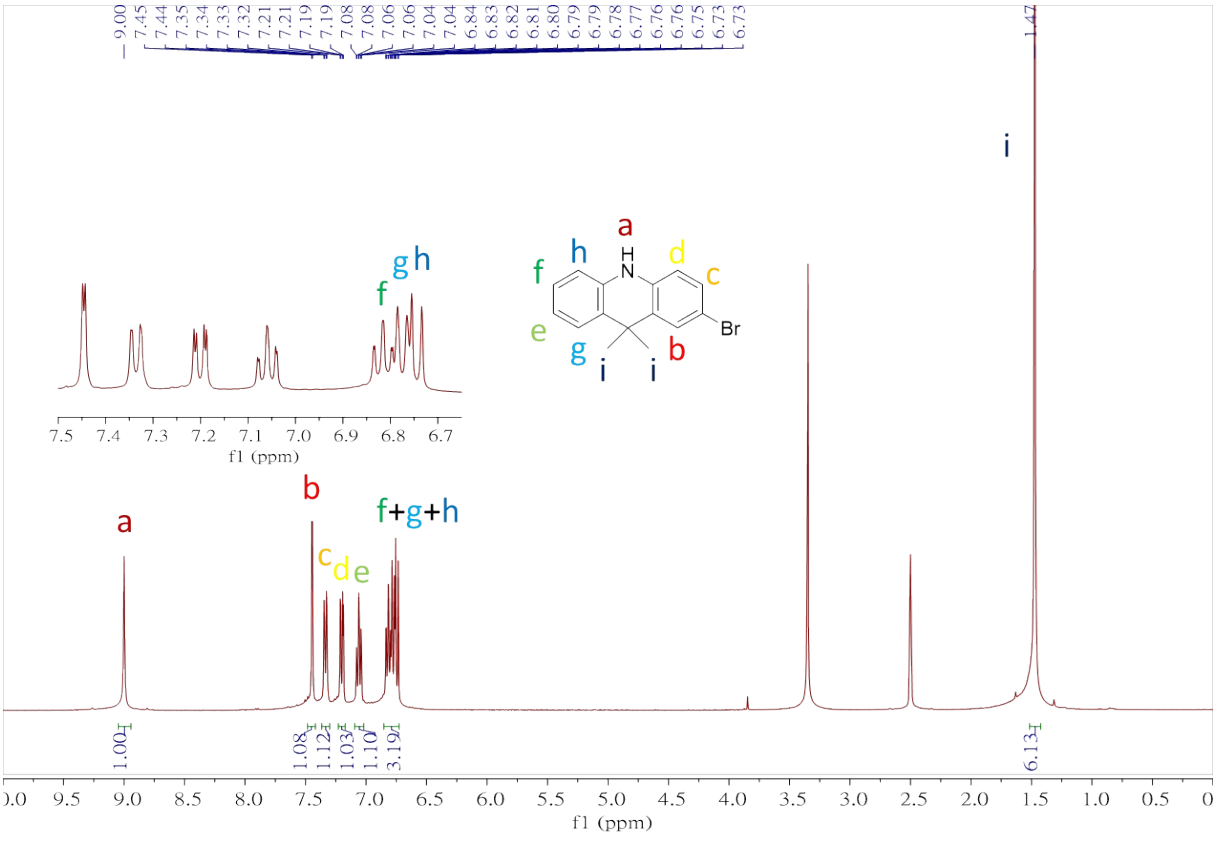

^{13}C NMR of compound **7**

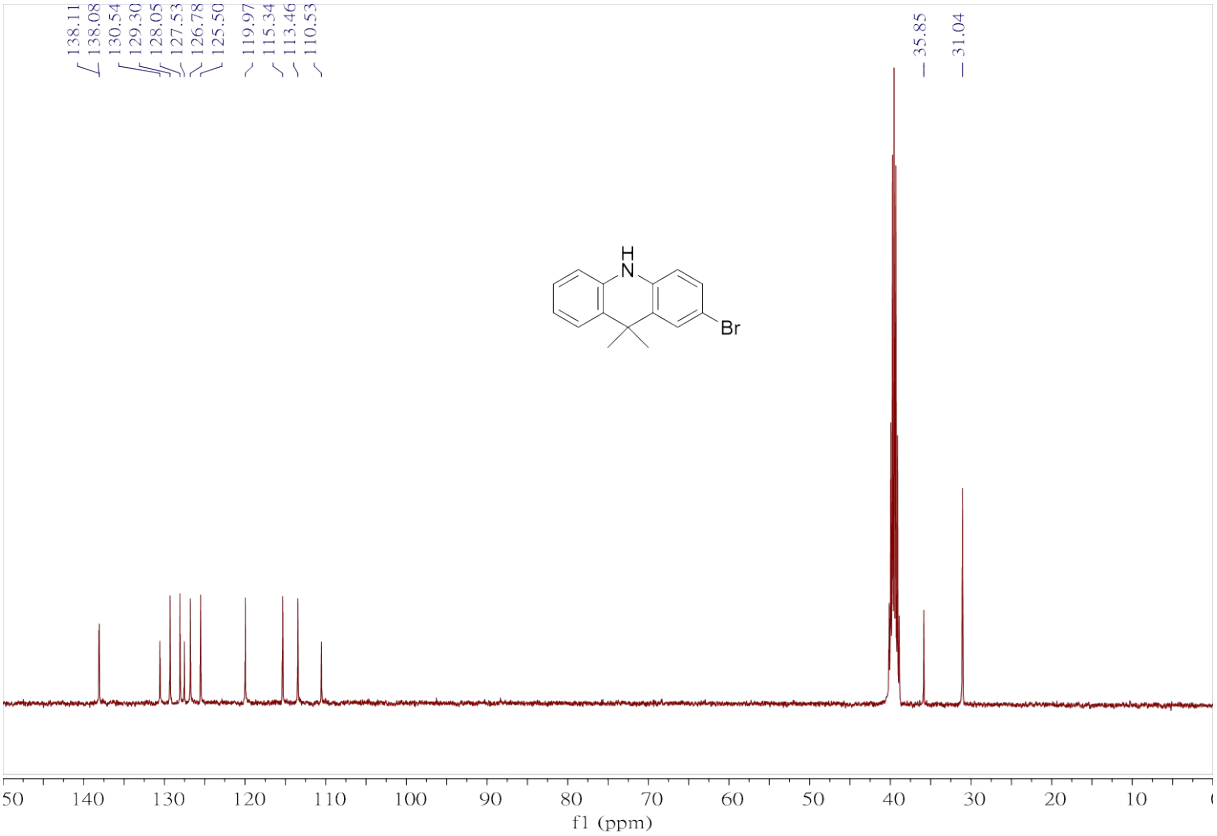

HR-Mass of compound **7**

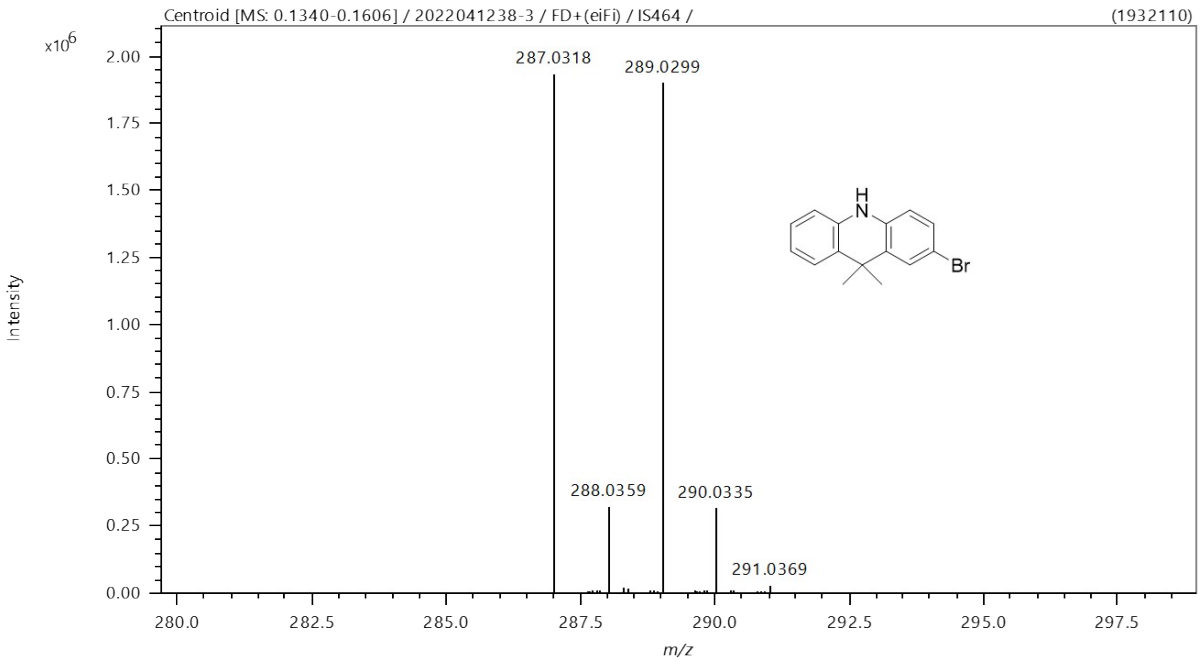

^{1}H NMR of compound **T1**

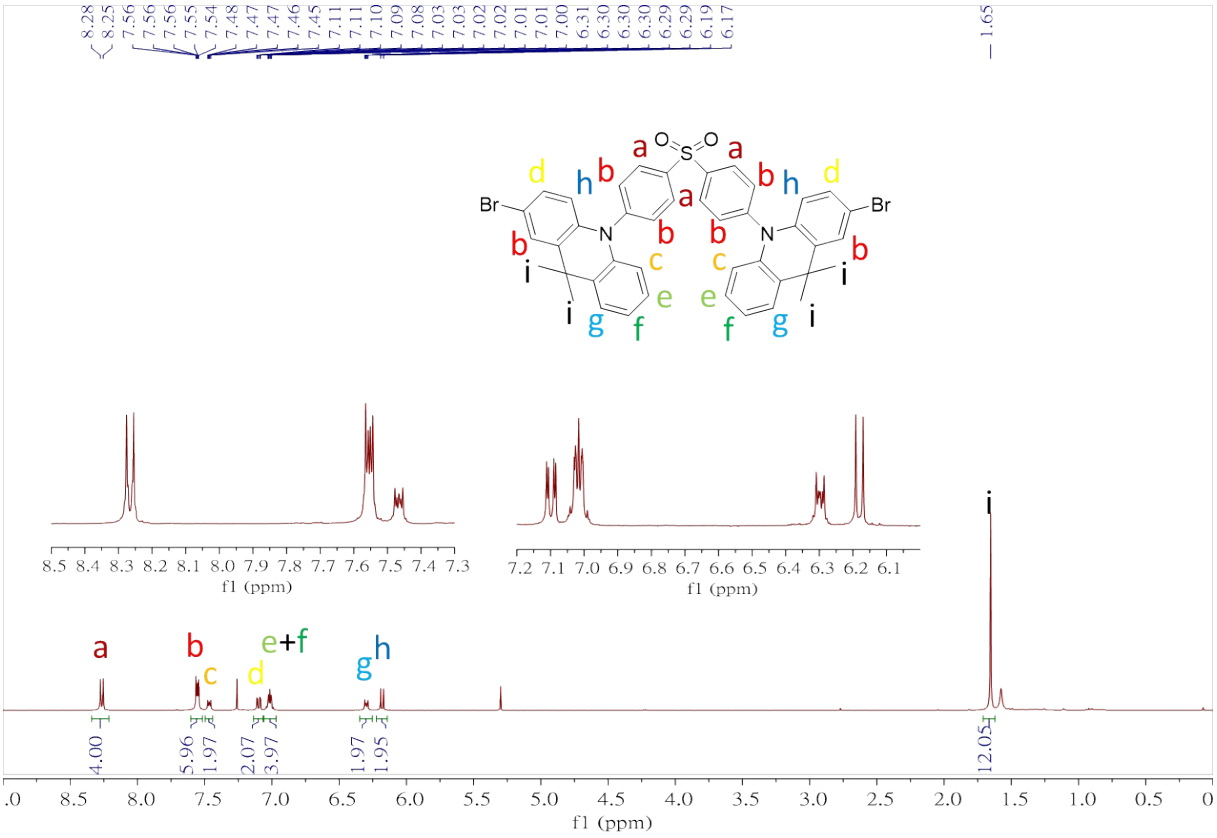

^{13}C NMR of compound **T1**

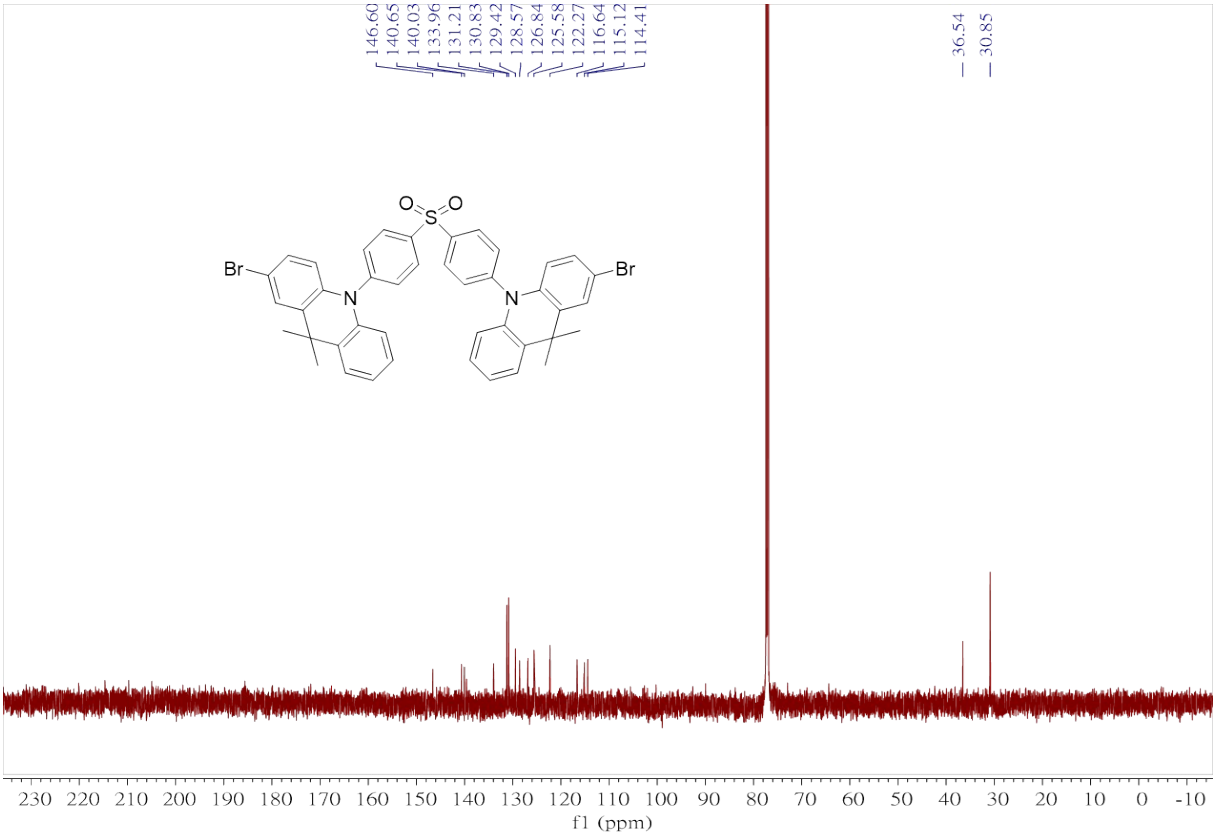

HR-Mass of compound **T1**

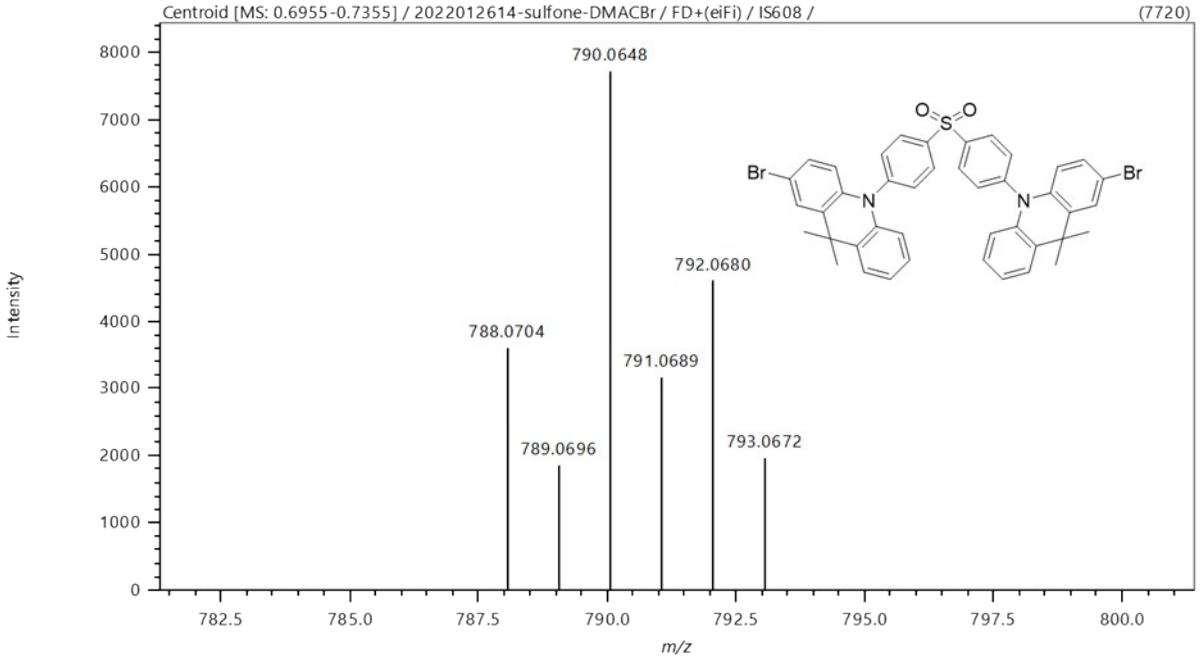

^{1}H NMR of compound **8**

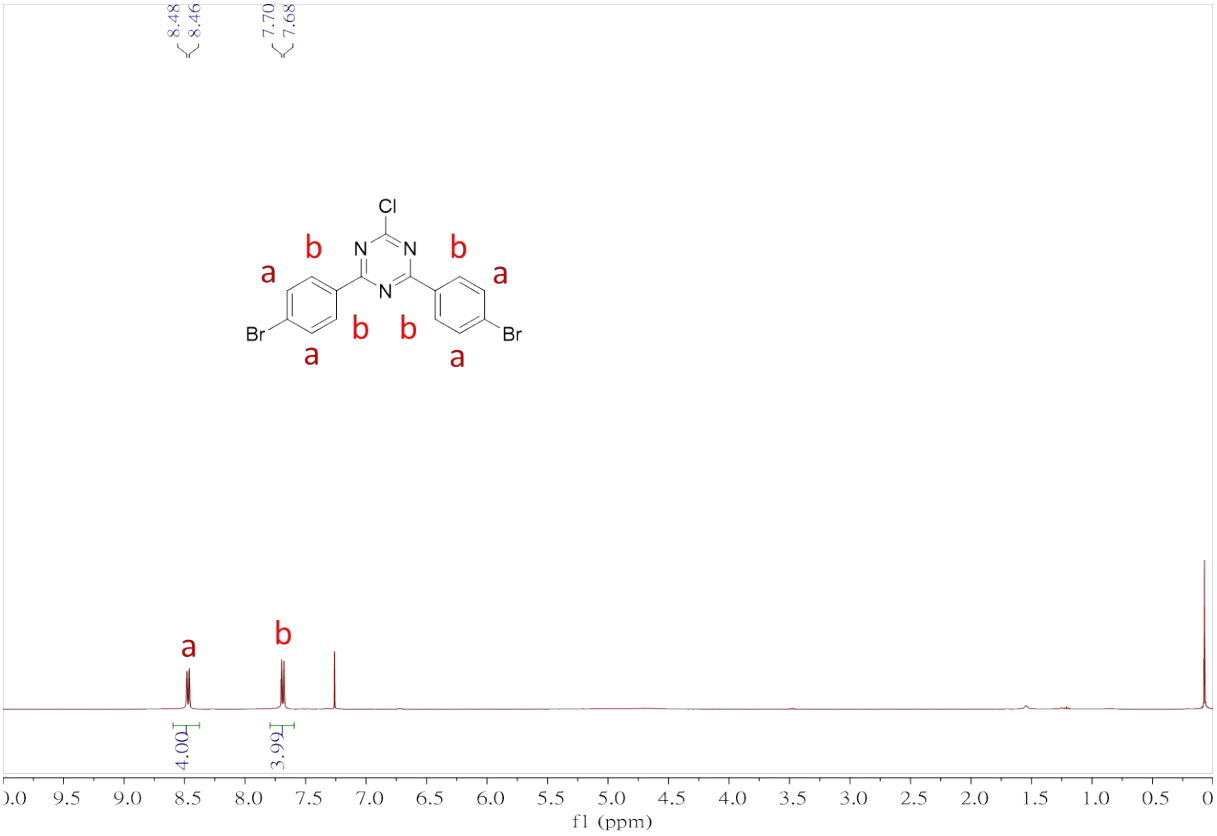

^{13}C NMR of compound **8**

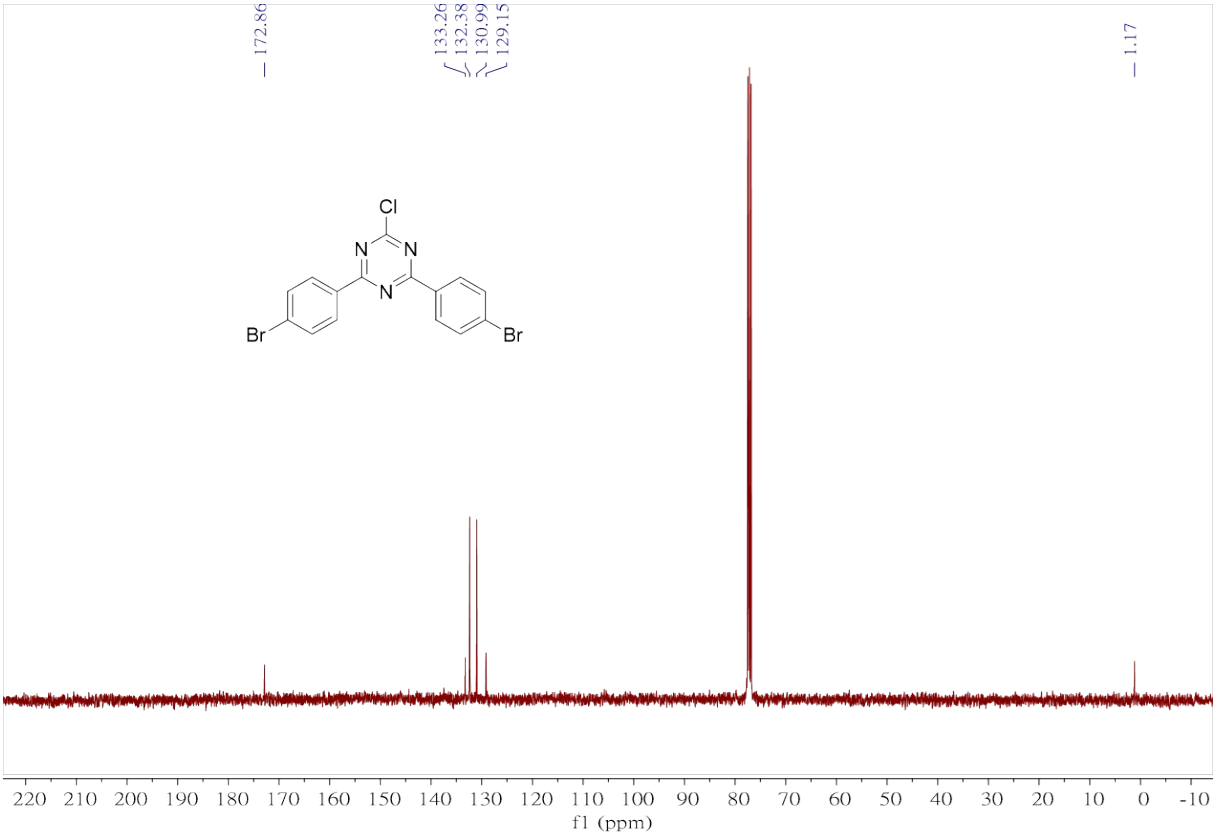

HR-Mass of compound **8**

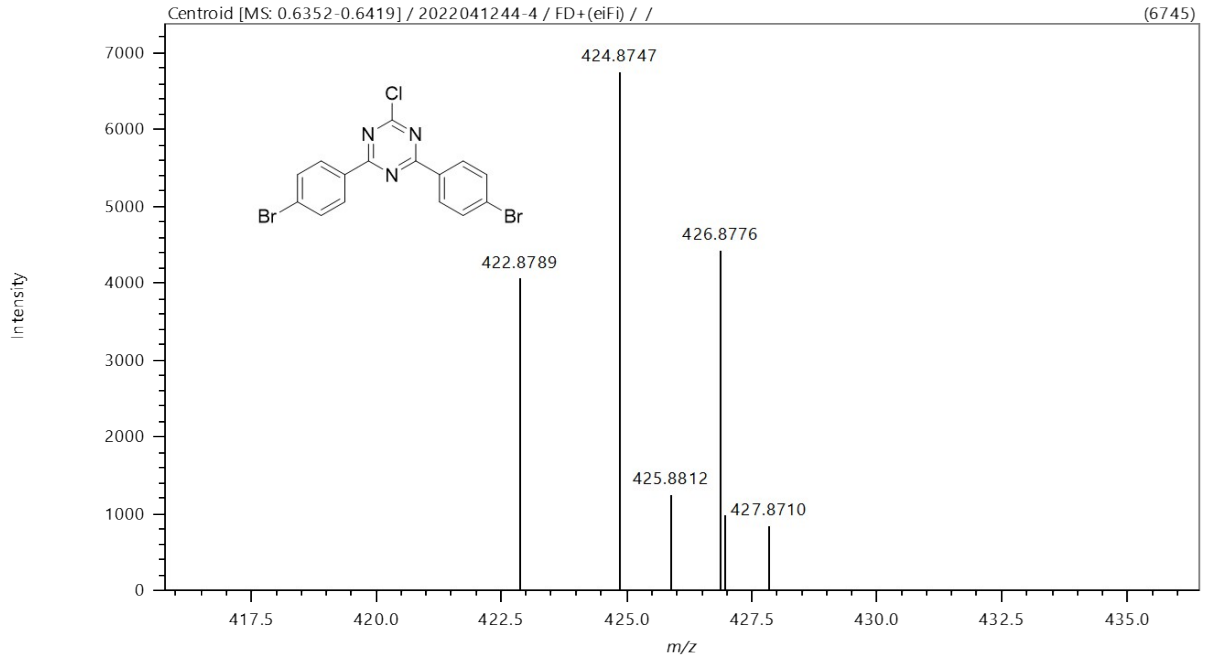

^{1}H NMR of compound **10**

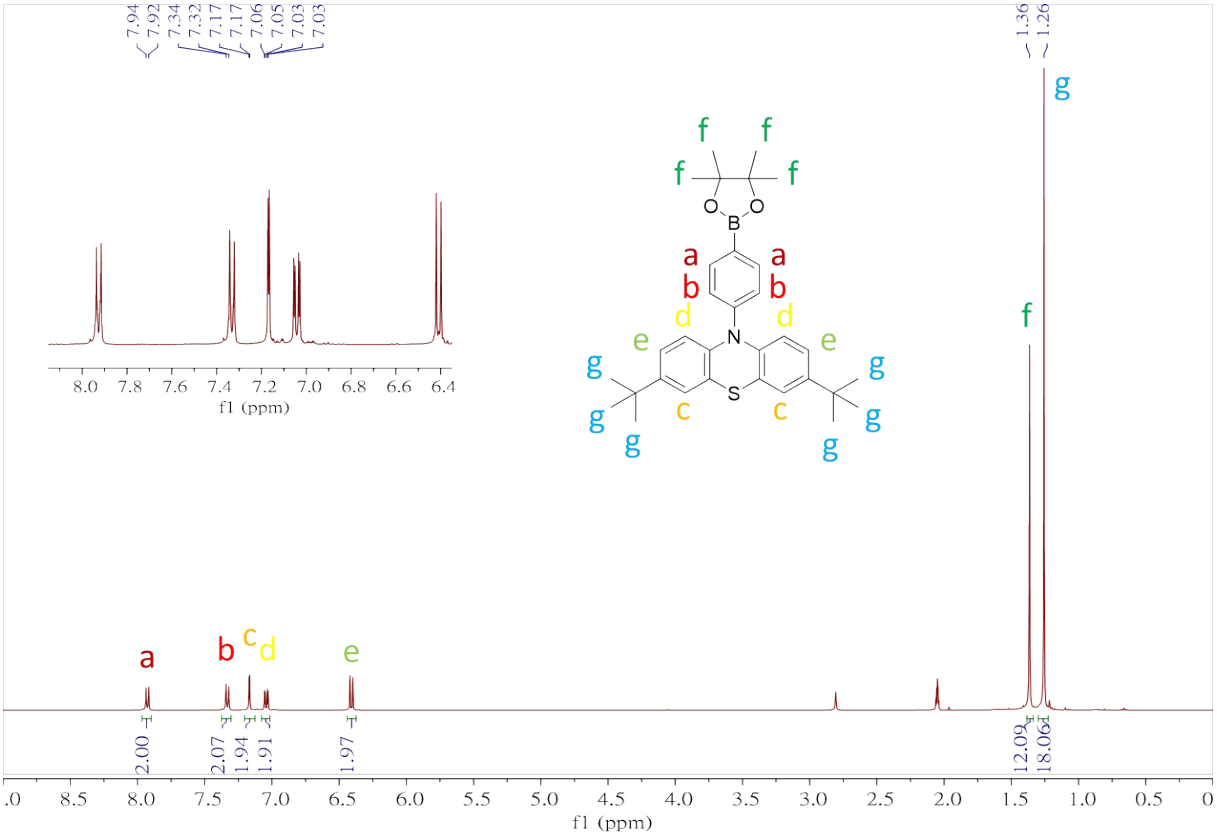

^{13}C NMR of compound **10**

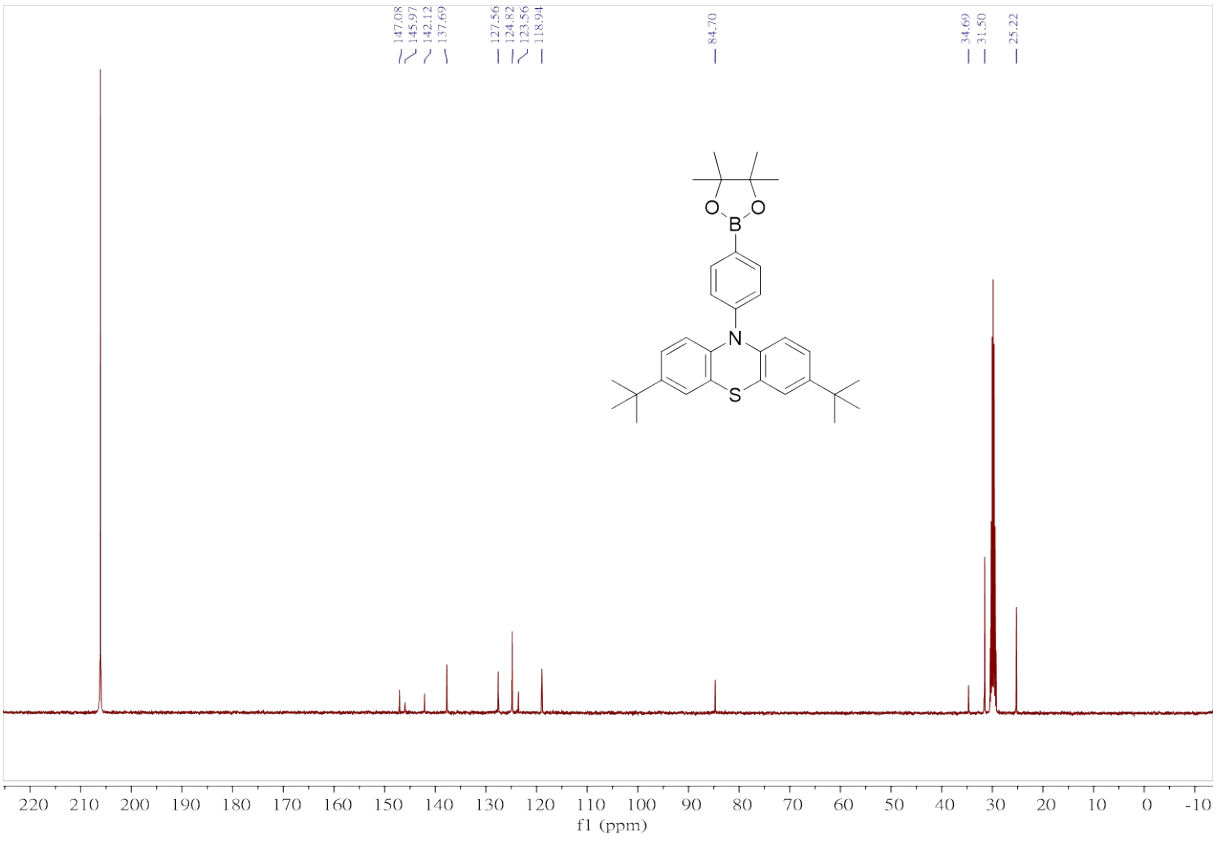

HR-Mass of compound **10**

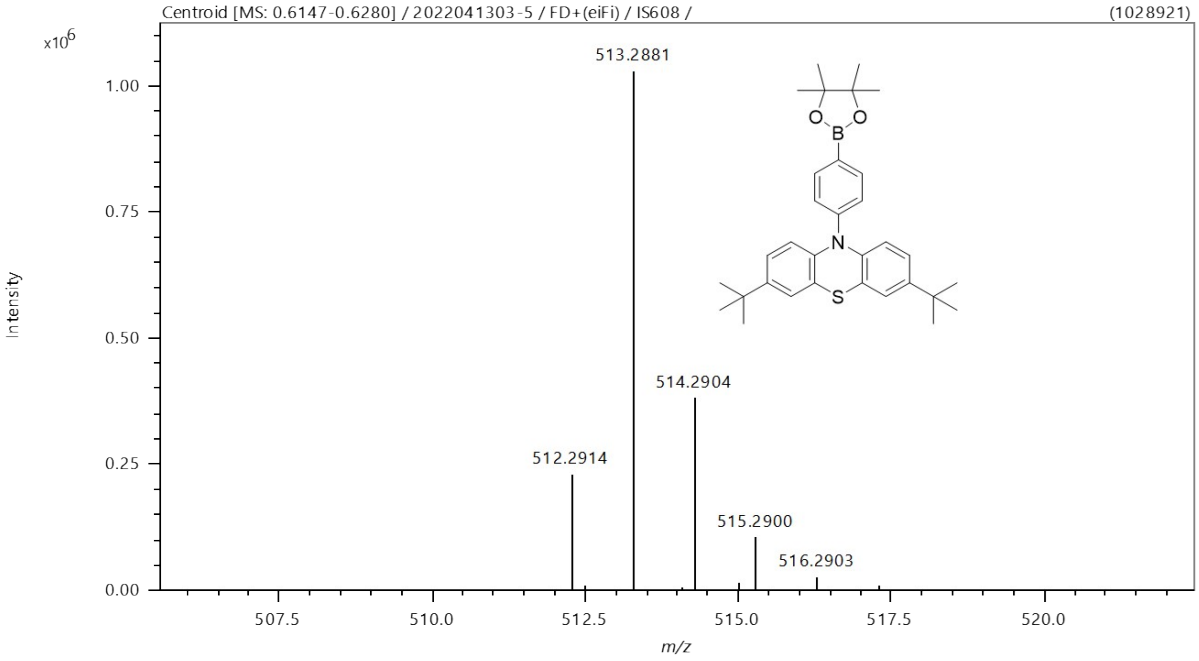

^{1}H NMR of compound **T2**

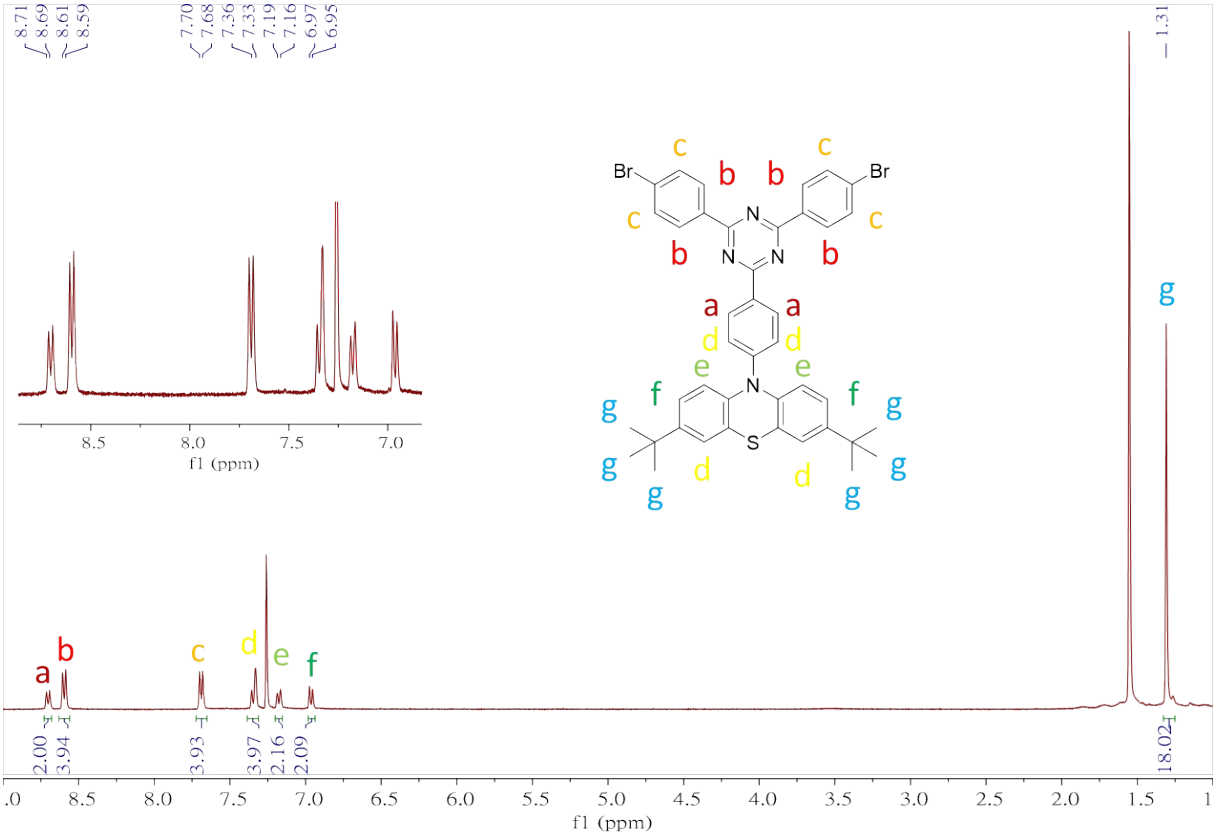

^{13}C NMR of compound **T2**

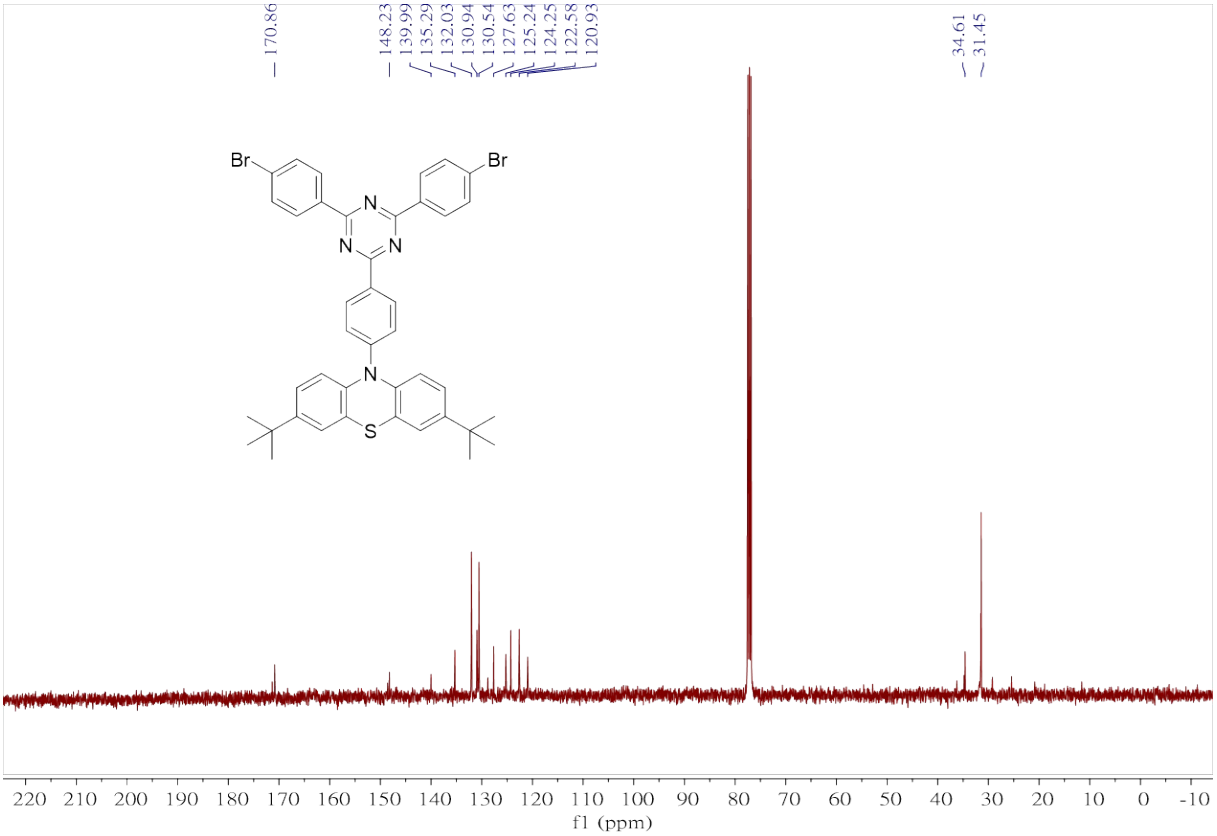

HR-Mass of compound **T2**

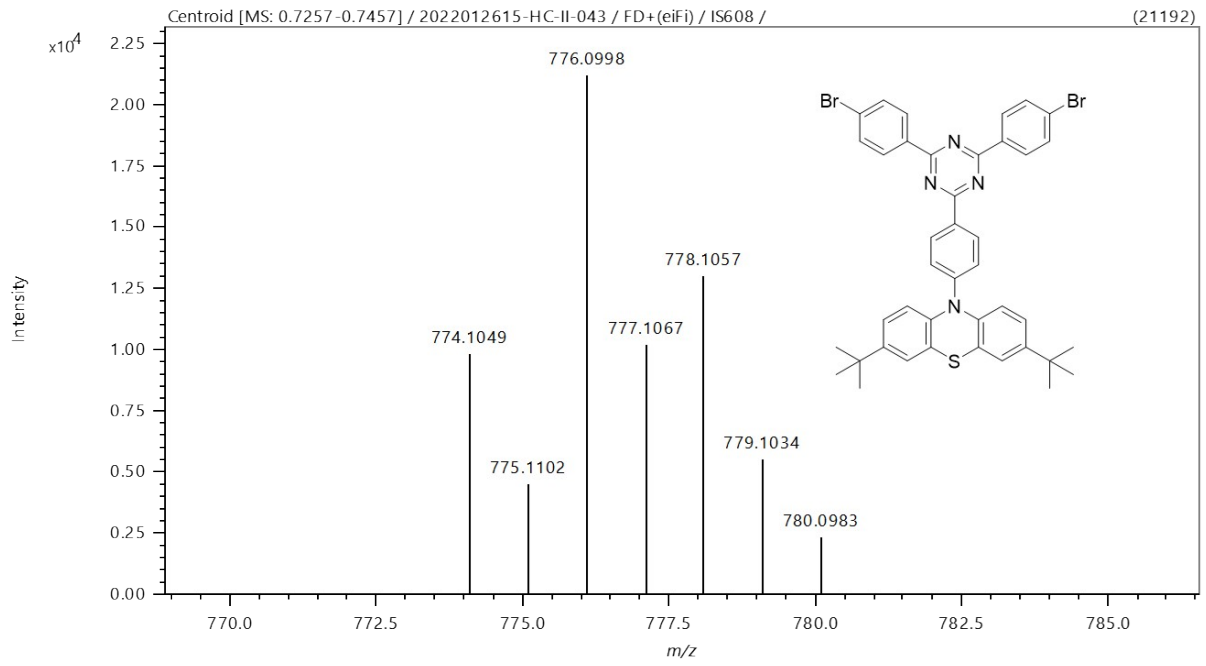

^{1}H NMR of compound **T3**

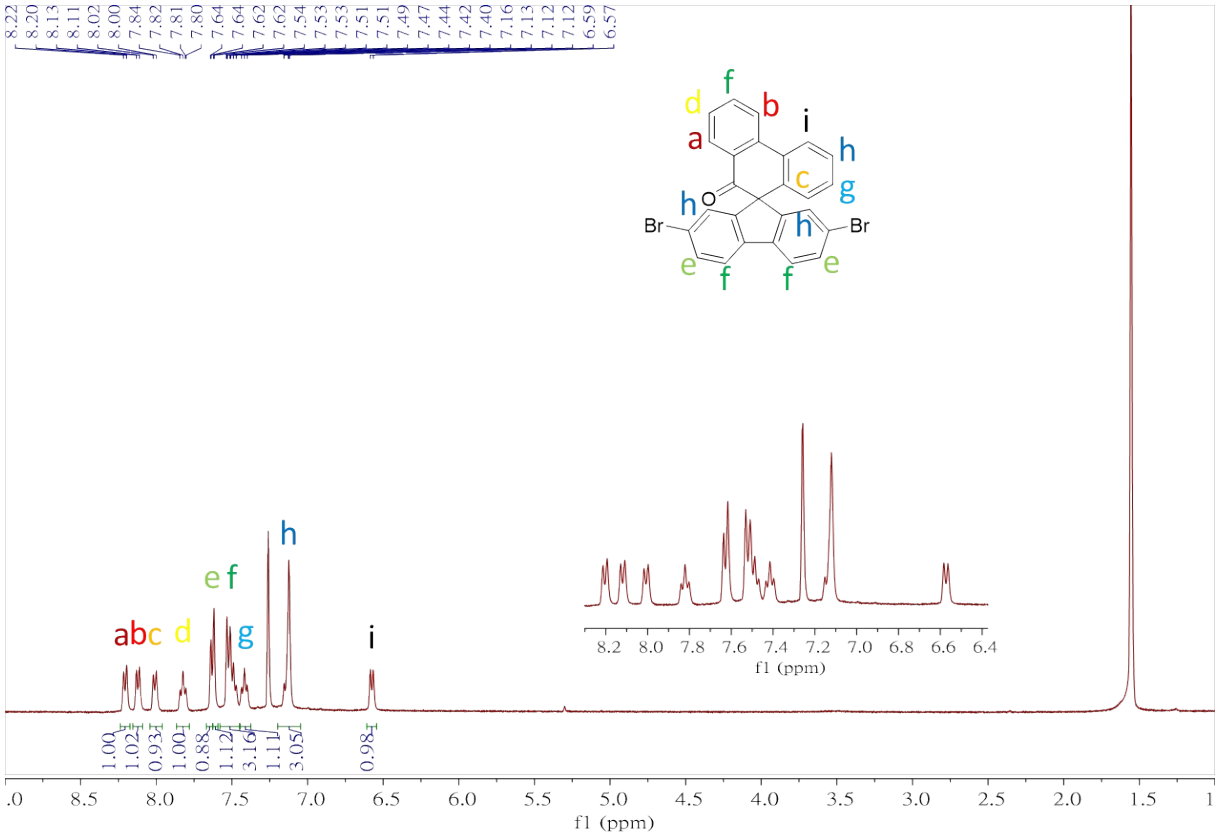

^{1}H NMR of compound **T4**

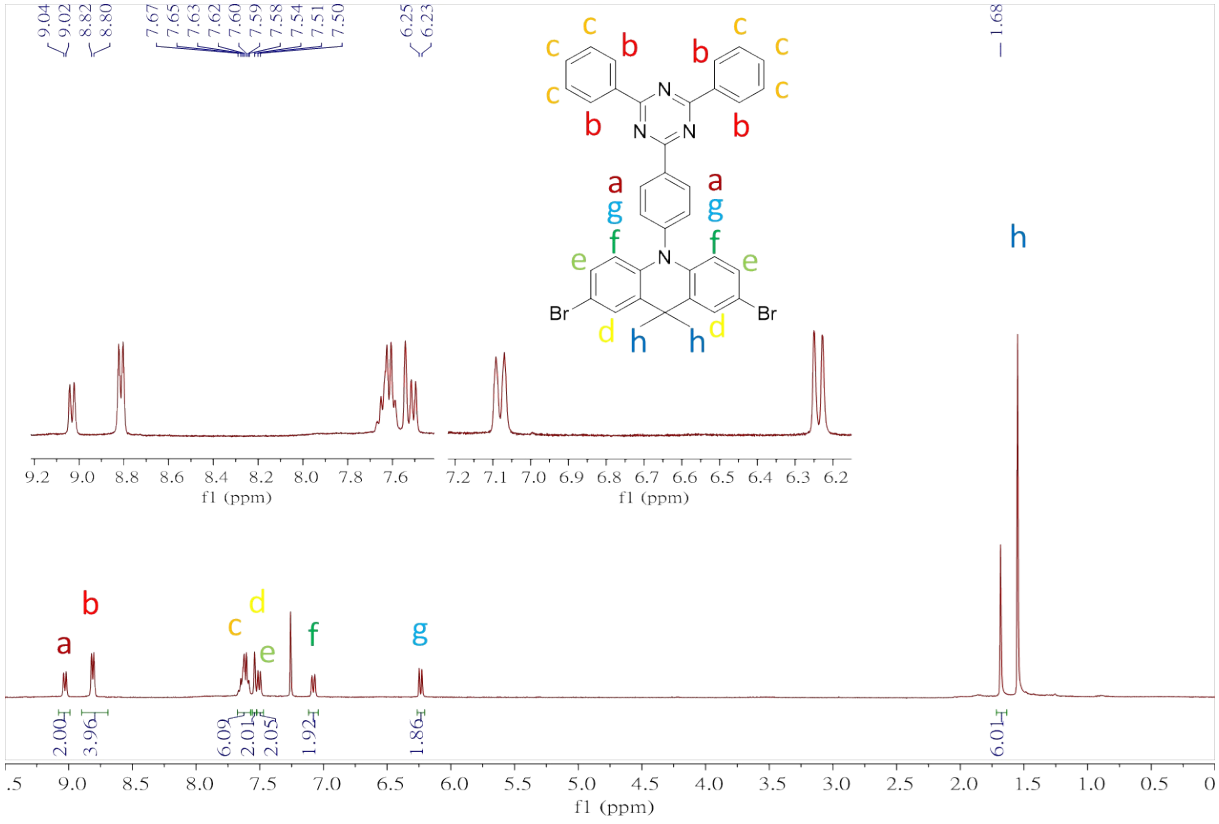

Supplementary References

1. M.-H. Liu, T.-C. Chen, J. R. Vicente, C.-N. Yao, Y.-C. Yang, C.-P. Chen, P.-W. Lin, Y.-C. Ho, J. Chen, S.-Y. Lin and Y.-H. Chan, *ACS Appl. Bio Mater.*, 2020, **3**, 3846-3858.
2. S.-H. Lee, C. T.-L. Chan, K. M.-C. Wong, W. H. Lam, W.-M. Kwok and V. W.-W. Yam, *J. Am. Chem. Soc.*, 2014, **136**, 10041-10052.
3. Y.-C. Chen, S.-K. Huang, S.-S. Li, Y.-Y. Tsai, C.-P. Chen, C.-W. Chen and Y. J. Chang, *ChemSusChem*, 2018, **11**, 3225-3233.
4. M. Godumala, S. Choi, H. J. Kim, C. Lee, S. Park, J. S. Moon, K. S. Woo, J. H. Kwon, M. J. Cho and D. H. Choi, *J. Mater. Chem. C*, 2018, **6**, 1160-1170.
5. M. Casalboni, F. De Matteis, P. Prosposito, A. Quatela, F. Sarcinelli, *Chem. Phys. Lett.*, 2003, **373**, 372-378.
6 Trani, F.; Scalmani, G.; Zheng, G.; Carnimeo, I.; Frisch, M. J.; Barone, V. *J. Chem. Theory Comput.* **2011**, *7*, 3304–3313.
7 Barone, V.; Cossi, M. *J. Phys. Chem. A* **1998**, *102*, 1995–2001.
8 Cossi, M.; Rega, N.; Scalmani, G.; Barone, V. *J. Comput. Chem.* **2003**, *24*, 669–681.
9. Gaussian 16, Revision A.03, Frisch, M. J.; Trucks, G. W.; Schlegel, H. B.; Scuseria, G. E.; Robb, M. A.; Cheeseman, J. R.; Scalmani, G.; Barone, V.; Petersson, G. A.; Nakatsuji, H.; Li, X.; Caricato, M.; Marenich, A. V.; Bloino, J.; Janesko, B. G.; Gomperts, R.; Mennucci, B.; Hratchian, H. P.; Ortiz, J. V.; Izmaylov, A. F.; Sonnenberg, J. L.; Williams-Young, D.; Ding, F.; Lipparini, F.; Egidi, F.; Goings, J.; Peng, B.; Petrone, A.; Henderson, T.; Ranasinghe, D.; Zakrzewski, V. G.; Gao, J.; Rega, N.; Zheng, G.; Liang, W.; Hada, M.; Ehara, M.; Toyota, K.; Fukuda, R.; Hasegawa, J.; Ishida, M.; Nakajima, T.; Honda, Y.; Kitao, O.; Nakai, H.; Vreven, T.; Throssell, K.; Montgomery, J. A., Jr.; Peralta, J. E.; Ogliaro, F.; Bearpark, M. J.; Heyd, J. J.; Brothers, E. N.; Kudin, K. N.; Staroverov, V. N.; Keith, T. A.; Kobayashi, R.; Normand, J.; Raghavachari, K.; Rendell, A. P.; Burant, J. C.; Iyengar, S. S.; Tomasi, J.; Cossi, M.; Millam, J. M.; Klene, M.; Adamo, C.; Cammi, R.; Ochterski, J. W.; Martin, R. L.; Morokuma, K.; Farkas, O.; Foresman, J. B.; Fox, D. J. Gaussian, Inc., Wallingford CT, 2016.
10 Martin, R. L. *J. Chem. Phys.* **2003**, *118*, 4775-4777.
11 Jelley, E. E. *Nature* **1936**, *138*, 1009–1010.
12 Würthner, F.; Kaiser, T. E.; Saha-Möller, C. R. *Angew. Chem. Int. Ed.* **2011**, *50*, 3376–3410.
13 Wang, Y. J.; Li, Z.; Tong, J.; Shen, X. Y.; Qin, A.; Sun, J. Z.; Tang, B. Z. *J. Mater. Chem. C* **2015**, *3*, 3559–3568.